CMS Tracking Simulation Studies
Final report

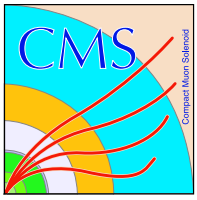

12 May 2008

Supervisor: Professor Geoffrey Hall

—

Henning Kirschenmann
3rd/4th Year Occasional Student
Imperial College / University of Hamburg
Email: hk07@ic.ac.uk; hkirsche@physnet.uni-hamburg.de

Contents

Chapter 1

Introduction

In this report the results of the two-term project "CMS Tracking Simulation Studies" will be presented. The Large Hadron collider at CERN will start operations this summer. When the first proton-proton collisions take place, the CMS-detector (Compact Muon Solenoid) will start taking data and allow the physics community to gain an understanding of the underlying physics of these collisions. Known processes will form a large background signal for the interesting new physics that can only be observed at the high energy scale of the LHC. The nature of the background signals - minimum bias events - and their impact on the tracker system of CMS will be discussed in the report. Depending on the character of these signals the occupancy in the barrel layers of the silicon strip detector can vary. The occupancy may not be too high in order to be able to reconstruct reliably what happened in the initial collisions.
Before the LHC goes into service only simulations and calculations can help to predict the conditions in the CMS tracker. There is already complex simulation software available for this purpose that can be used to estimate the occupancy. The complexity of the simulations is an advantage on the one hand, but on the other hand the validity of results becomes more and more difficult to assess. In order to get a better understanding of the occupancy results the origin of hits in the tracker of CMS causing this occupancy will be discussed in the report as well.

In the chapters 2 and 3 a general introduction to the particle accelerator Large Hadron Collider (LHC) and the general purpose detector Compact Muon Solenoid (CMS) will be given, section 3.2 describes the tracker of CMS in detail. Chapter 4 focuses on the simulation of the tracker by the CMS software.
In chapter 5 the origin of tracker hits will be discussed and estimations for the occupancy will be given.

Chapter 2

LHC

The Large Hadron Collider or LHC is a particle accelerator at CERN, the European laboratory for particle physics. The intended centre of mass energy of 14 TeV for the collision of two 7 TeV proton beams means a significant increase in comparison to all previously built storage rings (see fig. 2.1 for a Livingston-Plot).

2.1 Predecessors

2.1.1 Tevatron

The Tevatron at the Fermilab[1] can be seen as the predecessor of the LHC as a hadron collider. Beams of protons and antiprotons are accelerated to 980 GeV each and collide in the CDF and DØ detectors with a centre of mass energy of about 1.96 TeV. In 1995 the discovery of the top quark was announced and the observation of oscillations of B_S-mesons[2] was confirmed in 2006. When LHC is in full operation it extends the possibilities for research previously carried out at the Tevatron and the Tevatron will probably be shut down, then.

2.1.2 LEP

The LHC complex utilizes the tunnel (built 1983-1988) and various other facilities previously used by LEP, the Large Electron-Positron Collider. LEP

[1] The term "Fermilab" refers to the Fermi National Accelerator Laboratory in Batavia, Illinois

[2] Mesons are compound particles consisting of two quarks (one quark and one antiquark to neutralize the color charge of the quarks). The most familiar mesons are pions(π^+: $u\bar{d}$, π^0: $d\bar{d}/u\bar{u}$ and π^-: $d\bar{u}$) and kaons(K^+: $u\bar{s}$, K^0: $d\bar{s}/s\bar{d}$ and K^-: $s\bar{u}$).

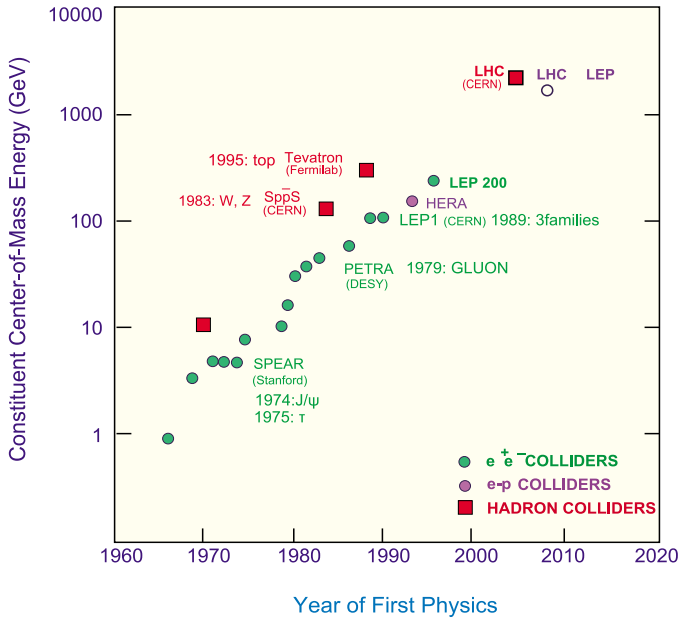

Figure 2.1: The Livingston-Plot shows the history in the development of particle accelerators beginning with fixed target experiments in the 1930s and relating today's collision experiments to the equivalent energy of fixed target experiments. [11]

operated from 1989 until 2000 and several important results have been obtained during the runtime: The mass of the W- and Z-Bosons were determined with great precision as well as the number of light neutrinos was constrained to three by the four complementary detectors Aleph, Delphi, Opal, and L3 built for the LEP. [4] The results obtained at LEP confirmed the validity of the "Standard Model" of particle physics and are the starting point for the physics programme at the LHC. After the operation of the LEP was shut down, the reconstruction for the LHC began.

2.2 Storage Ring

2.2.1 General

The storage ring of the Large Hadron collider is about 27 kilometres in circumference (compare fig. 2.2 for an overview) and between 50 and 150 m below ground crossing the Swiss/French border twice near Geneva. For some key parameters of the accelerator components see table 2.1. More than 1600 superconducting magnets are installed to keep the two proton beams in the desired direction.

Key parameters of the LHC	
Circumference	26.659 km
Centre of Mass Energy(protons)	14 TeV
Centre of Mass Energy(ions)	1150 TeV
Peak luminosity	$10^{34} cm^{-2} s^{-1}$
Number of filled bunches	2808
Number of particles per bunch	$1.5 \cdot 10^{11}$
Average bunch length (collision)	7.6 cm
Stored energy per beam(collision)	362 MJ
RMS beam size at CMS interaction point	16.7 μm
Collision rate	40 MHz

Table 2.1: LHC Key parameters with data taken from the LHC TDR Volume 1 [1]

2.2.2 Beam handling

Because of the densely packed bunches of high energy particles, special care has to be taken not to let the beam touch the beam pipe. There is a beam dump system installed at LHC point 6 (compare to the LHC Technical Design Report, Chapter 17 [1]) to dispose of the the high energy beam in a safe way. In order to eject the beam out of the usual circular motion there are kicker magnets installed to redirect the beam when it is due to be dumped. To be able to do this in a safe way there needs to be a pause between filled bunches. The neccessity of this pause is one of the reasons, why only 2808 of the 3564 bunches circulating in the storage ring are filled. Before the proton beams can be injected into the LHC they are preaccelerated in the Linac 2, PSB, PS and SPS (compare figure 2.2 for details). When running as an ion collider the acceleration chain is Linac 3, LEIR, PS and SPS.

2.3 Other Experiments than CMS

2.3.1 ALICE, LHCf, LHCb, TOTEM

Several detectors have been planned for the physics programme of the LHC. CMS (Compact Muon Solenoid) and ATLAS (A Toroidal LHC ApparatuS) are universal detectors and as such the largest. ALICE (A Large Ion Collider Experiment) is intended to examine the results of the collision of heavy ions(Mostly lead atoms with a centre of mass energy of 5.5 TeV per nucleon - equivalent to 1150 TeV total ($m_{Pb} = 207u$)).

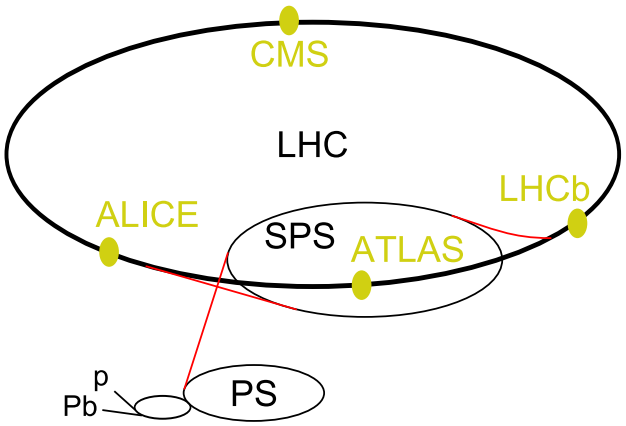

Figure 2.2: The LHC with experiments and its preaccelerators: Proton beams originate from the linear accelerator Linac 2 (50MeV) and are subsequently accelerated to 1.4 GeV (Proton Synchrotron Booster - PSB), 26 GeV (Proton Synchrotron - PS) and 450 GeV (Super Proton Synchrotron - SPS) before being injected into the LHC, where they are further accelerated to 7 TeV.

LHCb(Large Hadron Collider beauty) is intended to examine the interactions of b-mesons and b-hadrons and particularly the expected CP violation in these interactions. The LHCf(Large Hadron Collider forward) is split into two components, each 140 m from the ATLAS interaction point and measures the number and energy of neutral pions from collisions there. This is supposed to help explain the origin of very high energy cosmic rays. TOTEM(Total Cross Section, Elastic Scattering and Diffraction Dissociation) shares the interaction point with CMS and is - similar to LHCf - situated very near to the beam axis. Protons from elastic or quasi-elastic reactions with very low angles with reference to the beam axis will be detected as well as the overall rate of inelastic reactions for $3 < \eta < 7$ will be measured.

2.3.2 ATLAS

The CMS-detector will be covered in more detail in Chapter 3. The ATLAS-detector[6], however, is in terms of the physics programme quite comparable to CMS while the design differs in some aspects, so ATLAS's design will be covered here as well:

ATLAS consists of four major parts, the Inner Detector, the calorimeters, the muon spectrometers and the magnet systems. ATLAS is 46 metres long, has a diameter of 25 metres and weighs 7 000 tons (CMS: 21m long,

16 metres diameter, weight 12 500 tons). While the order of the tracking detector, calorimeters and muon tracking system is the same as for CMS, the magnet system design is significantly different in both detectors, allowing CMS its relatively compact size.
Surrounding the inner detector there is a solenoid producing a magnetic field of 2 Tesla. Built into the muon system there are eight superconductiong barrel loops and two endcap magnets producing a large, but not uniform, toroidal magnetic field.
The Inner Detector of ATLAS consists of three subsystems:

- A pixel detector with 3 barrel layers and 5 endcaps on each side covering a range of $\eta < 2.5$[3] with a total of 140 million channels
- A silicon strip detector with 4 barrel layers, 9 endcap wheels on each side and another 6.2 million channels
- A transition radiation tracker (TRT – 56 -107 cm from centre) using 50 000 straw detectors in the barrel (split in the middle) and 320 000 radial straws in the endcaps operating at a high occupancy, giving on average 36 measurements per track. There is no such system in CMS - it allows to cover a large volume at reasonable costs, but has only relatively few readout channels in return.

2.4 SLHC

The term SLHC (Super Large Hadron Collider) stands for various different proposals to increase the performance of the LHC after it has been running for several years and reached or even surpassed its design peak luminosity. As the time to halve statistical errors in measurements increases very soon after the LHC has started operation (compare fig. 2.3) and the accumulated integrated luminosity of the "design LHC" might not result in enough statistics for the discovery of some processes with very low cross sections (i.e. very rare), it is almost inevitable to change machine parameters instead of running with the same performance much longer.
As some of the components (especially of the tracking systems of CMS and ATLAS) will reach their lifetime after several years of operation, it is thought to be reasonable to combine the neccessary upgrade works at the detectors with an increased peak luminosity of $\mathcal{L} = 10^{35} cm^{-2} s^{-1}$. To avoid electron cloud effects in the machine a proposal has been made to reduce the bunch crossing frequency to 20 MHz, use slightly longer bunches and store more

[3] η, denotes the pseudorapidity defined as $\eta = -\ln\left[\tan\left(\frac{\theta}{2}\right)\right]$ with the polar angle θ. It is a convenient measure in hadron collider physics, because the particle production is roughly constant in a wide eta range in terms of $\frac{dN}{d\eta}$ and it is a lorentz invariant measure. η, ranges from infinity (parallel to the beam axis) to 0 (transverse to the beam axis) in this context.

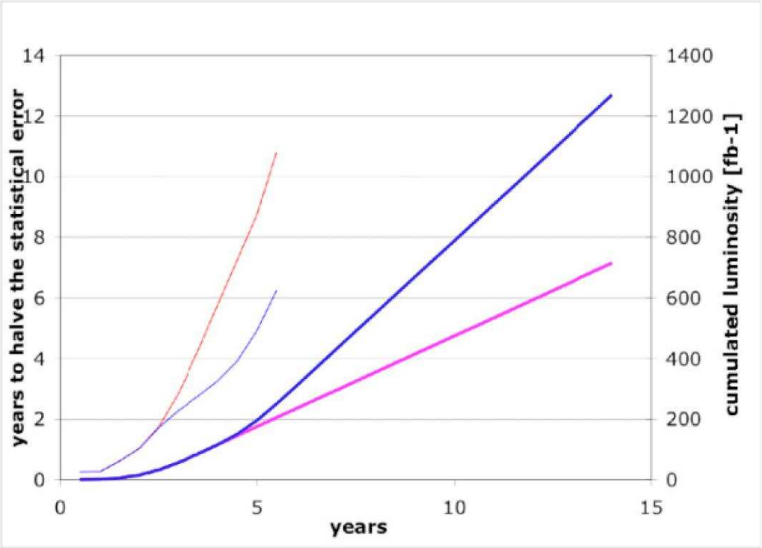

Figure 2.3: The graphs shows two potential running scenarios of LHC (1. achieving design luminosity after 3 years from startup; 2. achieving twice the design luminosity after 5 years). The left lines show the years to halve the statistical error, the right lines the cumulated luminosity.[7]

protons in each bunch. In every case the radiation doses in the environment of the interaction point and the number of tracks to be reconstructed will increase dramatically. There is already a lot of R&D being carried out for the redesign of components for the detectors to cope with the increased luminosity.

Chapter 3

CMS

3.1 Overview

The Compact Muon Solenoid is alongside ATLAS the other general purpose detector experiment at LHC. It has a total weight of 12500 tons, a length of 21.5 m and a diameter of 15 m. In figure 3.2 the essential setup of the detector is shown. Some of the main design concepts of the detector are represented in the name:

- *Compact:* The tracking system and all calorimeters are contained in a cylinder of 2.5 m diameter. Adding the solenoid, return yokes and muon chambers to the configuration increases the size significantly, but in comparison to ATLAS the detector covers only an eighth of the volume.

- *Muon:* Muons originate from the decay of heavier particles and are therefore a good indicator for interesting physics processes occuring in the interactions (e.g. some of the proposed decay modes of a Higgs with $m \geq 150GeV$). The massive amount of material between the interaction point and the muon chambers ensures that the signal in the muon chambers is in fact caused by muons and can be used for the Trigger System.

- *Solenoid:* CMS has a large superconducting solenoid at a radius of 3m covering the tracking system and calorimeters with a 4 Tesla magnetic field. Tracks of charged particles are bend strongly in the transverse plane - allowing for a precise momentum measurement together with the tracker data.

To be able to reconstruct the particles created in the collision of the proton beams (e.g. quarks and gluons composing the protons) it is important to determine energy, momentum and tracks of the observable particles precisely. If this information is obtained sufficiently accurate, it is possible

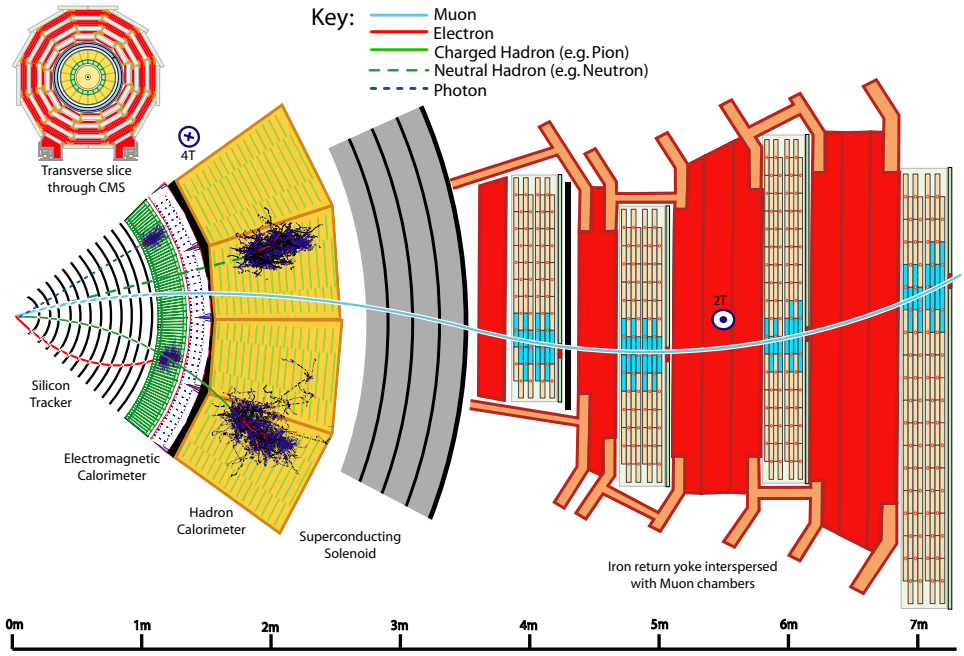

Figure 3.1: CMS-Slice

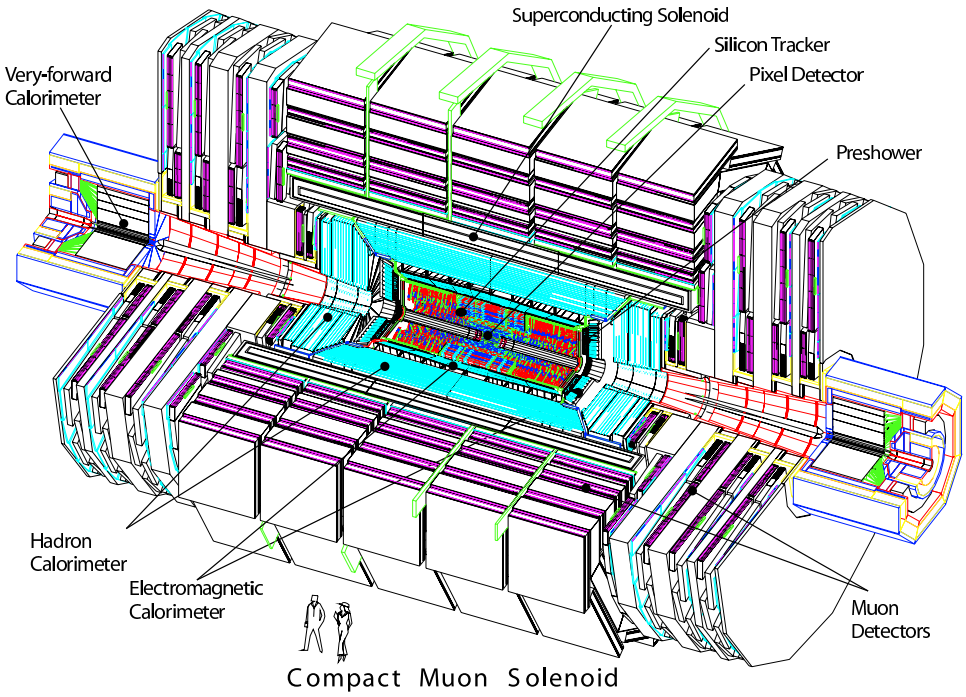

Figure 3.2: The whole apparatus

to reconstruct "missing" particles. "Missing" particles can either be quickly decayed particles resulting in the creation of particles then observable by the detector or particles that do not interact strongly enough with the material in the detector to be detected directly (e.g. Neutrinos, the Higgs and some proposed SUSY-particles[1]). In order to observe as many different particle types as possible in the detector there are different layers installed, each offering the ability to examine different classes of particles. For an illustration of the signals caused by different particles compare fig. 3.1.

1. *The Tracker:* The tracker consists of silicon sensors that are sensitive to charged particles. Reconstructing the signals caused by the particles passing through bent by the magnetic field gives access to their momenta and way through the detector (called the "track"). Compare 3.2 for more details.
   η-coverage(Pixel): $|\eta| < 3.0$; Silicon Strip: $|\eta| < 2.5$

2. *Electromagnetic Calorimeter(ECAL)[10]:* The ECAL main components are the 75848 scintillating Lead Tungstate crystals ($PbWO_4$), making the ECAL sensitive to photons and electrons facilitating a precise measurement of their energy. The ECAL will allow to distinguish between incoming single photons and pairs of photons from π^0-decays. Lead Tungstate has a high density ($8.3g/cm^3$), a short radiation length (0.89 cm) and a small Molière radius [2] [8] (2.2 cm), allowing a very compact calorimeter with a fine granularity. Silicon avalanche photodiodes in the barrel and vacuum phototriodes in the endcaps are used as photodetectors for the resulting shower of photons ($30\gamma/MeV$).
   η-coverage: $|\eta| < 3.0$

3. *Hadronic Calorimeter (HCAL):* The HCAL is sensitive to hadrons - in contrast to the silicon tracker including neutral hadrons. Similarly to the ECAL it measures the energy of the incident particles. It is divided into three parts: the barrel HCAL (HB), the endcap HCAL (HE) and the forward HCAL (HF). HB and HE are made of alternating layers of brass (50 mm) and plastic scintillator (4 mm), emitting light proportional to the energy of the incoming particle taht is detected by Hybrid photo diodes. The HF extends the sensitive region out to η<5

[1] SUSY = supersymmetric
The concept of Supersymmetry has been developed in the context of "Grand Unified Theories" trying to unify Electromagnetic, Weak and Strong interactions. Massive supersymmetric partners to all the known particles are predicted by these theories, but they have not been observed, yet (if they exist at all).

[2] The Molière radius scales with the radiation length as $R_m = 0.0265X_0 \cdot (Z + 1.2)$ and correlates with the transverse spread of electromagnetic showers, which are the signal causing processes in the ECAL. These electromagnetic showers are created by repeated pair production of photons and bremsstrahlung of incident electrons.

Radius (cm)	**Fluence of fast hadrons** ($10^{14} cm^{-2}$)	**Dose (kGy)**	**Charged Particle Flux** ($cm^{-2} s^{-1}$)
4	32	840	10^8
11	4.6	190	
22	1.6	70	$6 \cdot 10^6$
75	0.3	7	
115	0.2	1.8	$3 \cdot 10^5$

Table 3.1: Particle flux and radiation dose in the barrel part of CMS for $\int \mathcal{L} dt = 500 fb^{-1}$ [8]

and is needed for a good resolution of the missing energy.
η-coverage: $|\eta| < 5.0$

4. *Muon detectors:* The muon detector uses three different types of gaseous detectors to determine the muons and their momenta. The different types are deployed according to the expected particle flux and radiation (especially neutron) background. Drift tubes (DT) are installed in the barrel region, cathode strip chambers (CSC) in the endcaps and resistive plate chambers (RPC) in both parts.
The signal from the RPC is used for Level 1 trigger decisions and all the signals are used for a second momentum measurement of the muons. This second measurement after the one in the tracker is possible, because there is a strong magnetic field (2 Tesla) in the reverse direction of the solenoid's field induced by the return yokes in the muon chamber part.
η-coverage: $|\eta| < 2.4$

3.2 Tracker

The tracker is the part of CMS that is primarily designated for the determination of the way a particle is taking through the covered parts of the detector - called the track - and the momentum measurement of these particles.
In order to reconstruct a track, the hits in different layers must be linked to each other by software algorithms. The efficiency with which this will be carried out is illustrated in fig. 3.4. Once a track is reconstructed, this track can be analysed into further detail. As the strong magnetic field forces charged particles into a circular or spiralling movement with its radius proportional to the momentum of the particle, the momentum can be determined by ob-

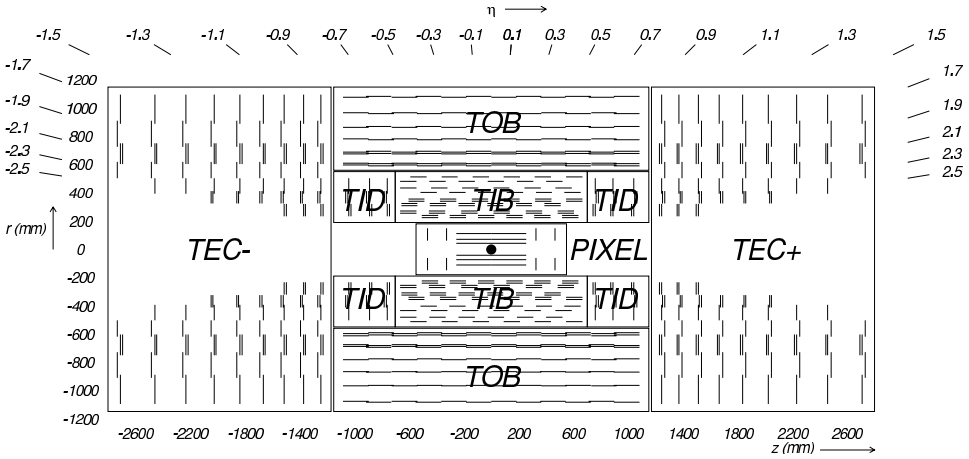

Figure 3.3: Layout of the Tracker in terms of η

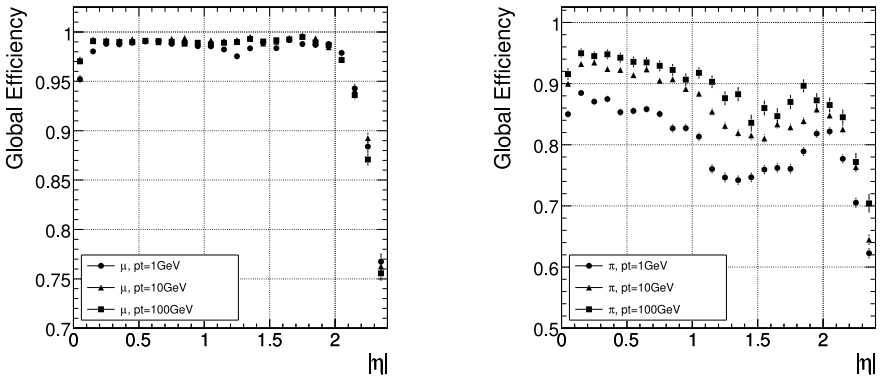

Figure 3.4: Track reconstruction efficiency for muons (left) and pions (right) of 1, 10 and 100 GeV/c transverse momentum[8]

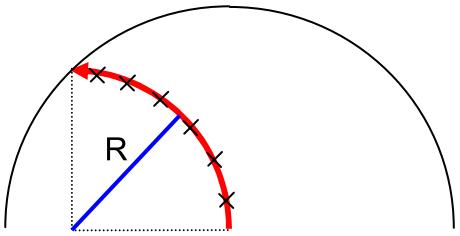

Figure 3.5: Determination of the momentum of a charged particle in the influence of a magnetic field.[12]

taining the radius of this spiral from the reconstructed track (compare 3.5).

$$\begin{aligned} \text{Lorentz Force:} |F| &= q \cdot B \cdot \frac{p}{m} \\ \text{Centripetal Force: } |F| &= \frac{p^2}{m \cdot r} \\ \Rightarrow p &= q \cdot B \cdot r \\ \text{In GeV units (and q=e): } p \left[\frac{GeV}{c}\right] &= 0.2998 \cdot r[m] \cdot B[T] \\ \text{with: } 0.2998 &= \frac{e \cdot c}{10^9} \end{aligned} \tag{3.1}$$

In fig. 3.3 the layout of the tracking system is shown. The tracker consists of several barrel and disk- or endcap-layers comprising silicon sensors. There are two general types of layers: Pixel- and Silicon Strip layers. As the particle and radiation flux differs considerably (compare tab. 3.1) depending on the radial distance from the interaction point (particularly due to the strongly bending magnetic field), these different types of silicon detectors had to be deployed.

3.2.1 Pixel Detector

The pixel detector of CMS is subdivided into the Pixel Barrel (PXB) and the Pixel Discs (PXD) and is situated next to the beam pipe and the interaction point. It has to withstand the harshest radiation conditions and even so be the detector part with the highest resolution and therefore the most channels. There are three barrel layers at radii of 4.4 cm, 7.3 cm and 10,2 cm, each 53 cm long. In addition there are two end disks at $\pm 34.5cm$ and $\pm 46.5cm$ from the interaction point, each extending from 6 to 15 cm in radius. Each pixel has a size of $100 \times 150 \mu m^2$ resulting in 65.9 million pixels in total.

3.2.2 Silicon Strip Detector

The silicon strip detector consists of four parts: the tracker inner barrel (TIB), the tracker outer barrel (TOB), the tracker inner disks (TID) and the tracker endcaps (TEC). It is situated outside of the pixel detector, stretches from r = 0.2 m to r = 1.1 m and has a total length of 5.5 m. There is a total of 9.6 million silicon strips in the strip detector. [13]
In the inner region (r < 55 cm) the modules have a minimum cell size of 10 cm × 80 μm, in the outer region (r > 55 cm) the maximum cell size can be extended to a maximum of 25 cm × 180 μm.
The TIB consists of 4 layers of silicon sensors with a thickness of 320 μm and a pitch between 80 and 120 μm. Layer 1 and 2 are stereo layers allowing measurement in the $r - \phi$ and $r - z$ coordinates. The TOB consists of 6

TIB Layer	Mean radius [mm]	No. of APVs	No. of Channels
1(DS)	255	4032	516096
2(DS)	340	5184	663552
3(SS)	415	2160	276480
4(SS)	500	2592	331776

Table 3.2: Key parameters of the Tracker Inner Barrel(TIB)

layers of 500 μm thick sensors. As the radiation level is significantly lower (compare tab. 3.1) as in the inner barrel layers, the strip pitch is ranging between 120 and 180 μm.
The silicon strip detector is operated at a temperature of -20^oC in order to keep the noise and radiation damages low. More detailled parameters of the TIB - the most examined region of the detector during this work - including the number of APVs are shown in tab. 3.2. APVs (for Analog Pipeline [Voltage Mode]) form the initial readout system of the CMS Tracker. 128 input channels are amplified and their signal is converted to about 50 ns wide voltage pulses, which are buffered in a 192 stage pipeline waiting for the trigger decision. The height of the pulse is proportional to the number of MIP equivalents hitting the sensor. MIP is the abbreviation for minimum ionizing particles - being those particles in the region with a minumum energy loss $\frac{dE}{dx}$ according to the Bethe-Bloch equation (compare formula 3.2).

3.2.3 Design of a microstrip detector

The essential design concept of a microstrip detector will be illustrated using fig. 3.6. The constituent components are diodes consisting of a p-(the strip) and a n-doted region. The n-doted region can be shared by many strips. The different doping results in an uneven distribution of the charges: electrons from the n-doped region diffuse to the p-doped region, holes vice versa. An electrical field builds up that stops further diffusion.
When ionizing (i.e. primarily charged) particles pass through the silicon they create electron-hole pairs along their way. The electrons and holes move in contrary directions due to their opposite charge and the electrical field in the diode. The more pairs are created, the higher the temporary current increase will be, that can be read out and forms the signal processed in the above mentioned APVs.
The energy loss by relatively heavy particles (electrons are excluded) is described by the Bethe-Bloch equation [4] as shown in eq. 3.2). This form is accurate to about 1 % for pions with energies between 6 MeV and 6 GeV passing through copper. Above this energy radiation losses become dominant, below this energy range there are extensions by Anderson-Ziegler and

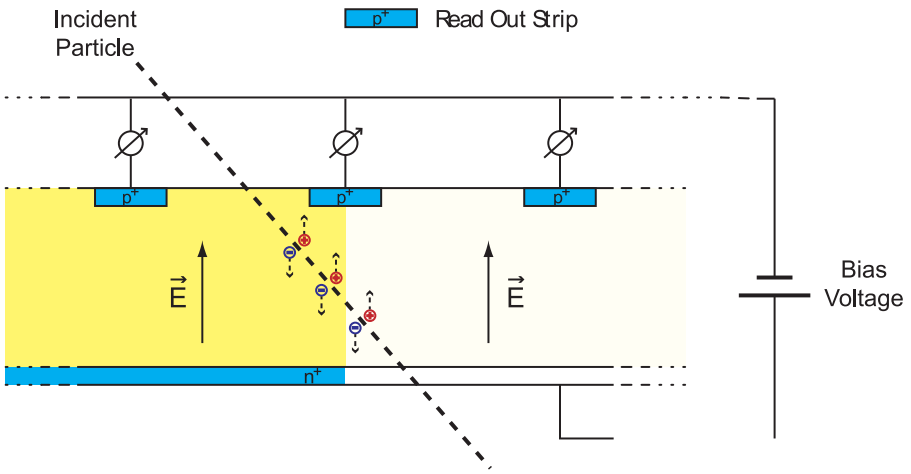

Figure 3.6: Working principle of a semiconductor detector [14]

Lindhard-Scharff. As the energy loss distribution with its long tail is a Landau distribution, the mean value as it is given by the Bethe-Bloch equation is significantly higher than the most probable energy loss.

$$\text{Bethe-Bloch:} \quad -\frac{dE}{dx} = Kz^2\frac{Z}{A\beta^2}\left[\frac{1}{2}\ln\left(\frac{2m_e c^2\beta^2\gamma^2 T_{max}}{I^2}\right) - \beta^2 - \frac{\delta(\beta\gamma)}{2}\right] \tag{3.2}$$

Low energy photons primarily loose energy by ionisation, but as the rate of this process rises only logarithmically in contrast to the rates of bremsstrahlung (which rise linearly), bremsstrahlung becomes the dominating process above several tens of GeV.
Depending on the the incident angle of the particle passing through the detector, more than one strip can collect charge deposited in the intermediate region. The detector response of the actual CMS detectors can be simulated within CMSSW [3] .

[3]CMSSW (CMS software) is the name for the overall collection of software - including the framework and the EDM(event data model) - used for the development of reconstruction and analysis software.

Chapter 4

Tracker Simulation - General

One of the main goals of the project is to carry out simulations of the tracker, gaining an understanding of the processes that the particles created at the interaction point experience. The examined particles originate from so called minimum bias events, which will be explained in section 4.1. When these particles propagate through the detector, they interact with the magnetic field and the material in the detector, unstable particles decay very fast. Depending on their lifetime semistable particles partially decay when passing through the detector, the remains of these decays propagate through the detector, too.
During the time of this project several approaches to data acquisition were undertaken. Minimum bias events were first generated using PYTHIA (see 4.2.2) and then analysed at this stage. GEANT4 (see 4.2.3) is used to simulate the further behaviour of the generated particles, their interactions with the material in the detector and the magnetic field and decays.
This raw data is used in the CMSSW-framework to simulate the response of the sensors and the readout electronics. Within the same framework the High Level Trigger response and the reconstruction and analysis of the data can be executed.

4.1 Minimum Bias events

Intensive studies about the nature of hadronic interactions have already been carried out and experimental data from previous collider experiments show that the most dominant signal from these collisions is characterized by low-p_t parton scatterings [1]. A typical frequent background interaction is shown in fig. 4.2. This schematic reaction is governed by the strong interaction,

[1] Parton is a term originally formed in the sixties to describe the constituents of hadrons. Later it was found that hadrons consist of quarks and gluons. The term refers here to both, quarks and gluons.

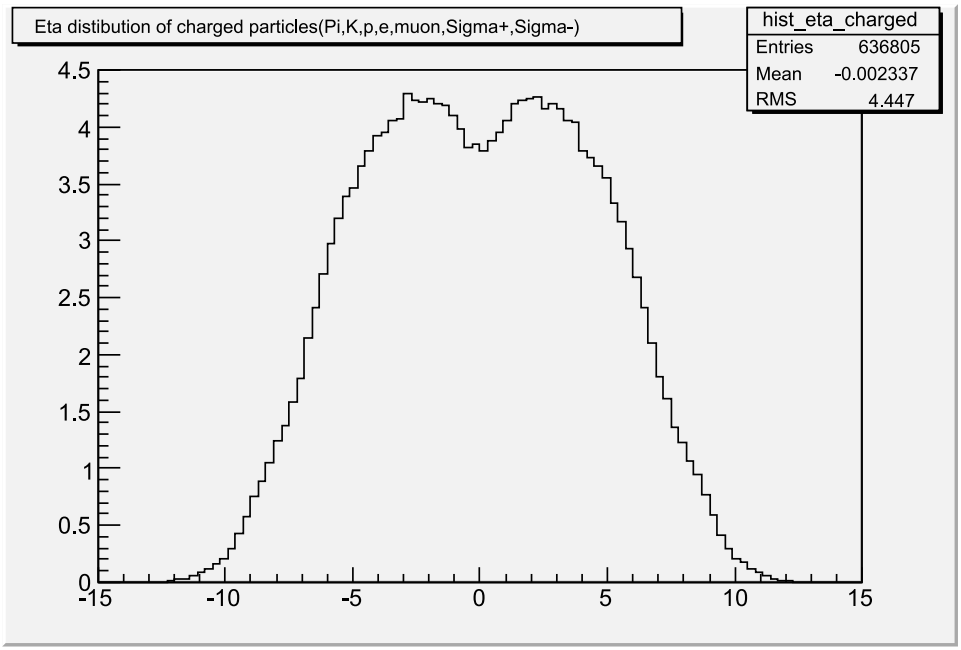

Figure 4.1: Charged particle density distribution $\frac{dN_{ch}}{d\eta}$ from the simulations, see appendix A for PYTHIA settings

described by the QCD [2] .
Collisions of hadrons with a high momentum transfer (hard collisions) between the interacting partons can be described successfully by pertubative QCD. However, most of the collisions are "soft" interactions with a low transverse momentum transfer. These soft interactions - so called non-single-diffractive reactions (NSD)[15] - are modelled in PYTHIA (compare section 4.2.2). PYTHIA attempts to extend the pertubative QCD to these low-pt transfer reactions. These models consider the possibility of multiple parton scattering taking place in these collisions. [23]
In fig. 4.1 the charged particle density distribution of the finally used dataset is shown, the minimum bias events were generated using PYTHIA 6.409 as shown in the appendix A. The resulting cross section of the simulation of min bias events is $\sigma = 79,19mb = 7,919 \cdot 10^{-30}m^2$. "Self simulated" events were used during the first time, but for final statistics a presimulated dataset taken from the LHC data repository was used.

[2]QCD: The theory of quantum chromodynamics describes the strong interaction, the fundamental force for the interation of quarks and gluons. It is described in the Lagrangian below and invariant under local SU(3) Gauge transformations. [25]

$$\mathcal{L}_{\mathrm{QCD}} = [i\hbar c\bar{\psi}\gamma^{\mu}(\lceil_{\mu})\psi - mc^2\,\bar{\psi}\psi] - \frac{1}{16\pi}F^{\mu\nu}F_{\mu\nu} - (q\bar{\psi}\gamma^{\mu}\lambda\psi)\cdot A_{\mu} \tag{4.1}$$

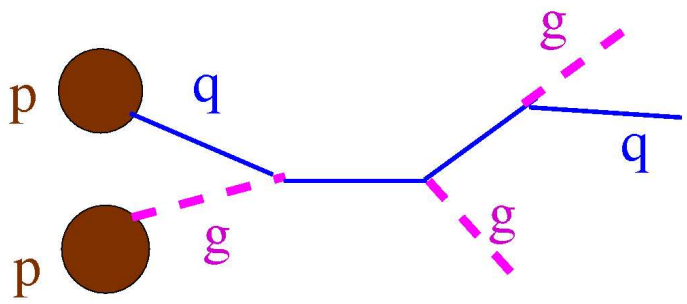

Figure 4.2: Example strong interaction background event at LHC[24]

4.2 Overview over different stages of the simulation

The first simulation stage using the event generator PYTHIA has just been mentioned in connection with the minimum bias events examined in this project. The generated particles are propagated through the detector and interactions with the material are simulated by GEANT4. From then on the CMSSW framework takes over the raw data and allows to carry out all further reconstruction and analysis. The data and results in all these steps is stored in .root container files.

4.2.1 Data format and analysis framework - ROOT

ROOT is a software package developed by CERN and is used for a wide variety of data analysis applications in particle physics. Data of all the different simulation stages and analysis results are stored in .root files that are suborganised into trees, branches and leaves. The TBrowser, part of ROOT, allows to navigate through this structure and to access e.g. histograms.
In this project the .root-files have been accessed in different ways during the subdivided simulation process. The output from the simulated collisions(PYTHIA) is stored into a .root-file. This output is read out and handed over to GEANT4 which simulates the detector and stores the new simulation data into another .root-file. At all stages the CMSSW-framework has access to the data and can perform subsequent simulation (see 4.2.4 for digitization) and analysis.

4.2.2 Simulation of collisions - PYTHIA

PYTHIA [20] is a program for the generation of high energy physics events. The collision of two incoming particles (e.g. e^-p, pp, $p\bar{p}$, e^+e^-) is simulated, including experimentally approved models for the interactions and various

extensions for physics processes beyond the standard model. It is the most commonly used Monte Carlo event generator in high energy physics. The generated particles originating from these collisions are stored in root-files as HepMC::GenEvent container class that can be accessed by the CMSSW-framework.
Within the GenEvent-class each separate particle is stored in the so called HEPMC::GenParticle class, that allows access to different properties of the particle, e.g. its momentum, its status (intermediate products are saved as well) and particle type. In 5.1 the statistics of (semi)stable particles is examined. Within PYTHIA the decay of particles with a very short lifetime, e.g. the π^0, is handled internally. They are not found as (semi) stable particles, only their decay products. These semistable and stable particles are saved with *status one* and handed over to the GEANT simulation.
PYTHIA can be configured with a wide range of different parameters. For the extrapolation to LHC energies there are different tuning parameters being discussed (e.g. those in [15]). We used the same parameters as they are used for the validation of new CMSSW-versions. The configuration file is shown in app. A.

4.2.3 Simulation of the particles' behaviour and interactions in the detector - GEANT4

GEANT4 (for GEometry ANd Tracking) by the GEANT4 Collaboration [21] is a program suite for the simulation of the passage of particles passing through matter. The geometry and material of the detector and the magnetic field is taken into account in order to simulate the tracks of particles propagating through. Interactions with the matter and decays are taken into account. Of particular importance is the energy loss that occurs when charged particles pass through the sensitive detector elements.

Simtracks

Simtracks are data objects in the simulation that have among others their source vertex, their particle type, charge and four momentum stored with them. They are constructed from primary particles from the PYTHIA-event generator and reference them or are created during the simulation within GEANT when interactions with matter or decays take place. Simtracks are only saved permanently when their momentum is above a certain threshold. This means that a "simhit", which will be explained next, has not always a track associated with it that has the same particle type. If the particle or simtrack causing the simhit has a momentum below 0.5 GeV the mother particle is referenced instead.

Simhits

Simhits are those data containers called that save the information that is generated, when a particle passes through a sensor module and interacts with the material there.

They have different properties saved with them:

- The DetId: Is a general variable that allows to decide in which detector part(e.g. Tracker or ECAL) the hit was generated and contains more detailed information about the part. E.g. for the PXB the information contains the ladder, layer and mudule, for TIB and TOB layer and module.
- The particle type: The type of the particle that caused the hit is saved in accordance to the PDG Monte-Carlo numbering scheme of the Particle Data Group. [4]
- The process type: The process type contains information about the process in which the particle that caused the hit was produced. A documentation for the categories can be found in the "Process/Model Catalog" at the GEANT collaboration homepage.[21] The definition from the Physics reference manual reads:

  > **process** - a C++ class which describes how and when a specific kind of physical interaction takes place along a particle track. A given particle type typically has several processes assigned to it. Occaisionally "process" refers to the interaction which the process class describes.

- The energy deposited in the detector unit that was hit in GeV.
- The entry point in the local coordinate system, the momentum at entry and the time of flight from the primary vertex.

4.2.4 Simulation of the detector response and analysis framework - CMSSW

CMSSW is a powerful framework (compare fig. 4.2.4 for a schematic overview) that is designed to incorporate the whole reconstruction and physics analysis. In addition it gives the opportunity to access and execute the event generator PYTHIA and the detector simulation GEANT.
Key component for users is the `cmsRun` executable. It is used by attaching a configuration file that calls for different modules and allows to configure them. Three types of modules have been used primarily in the project: "Source", "EDAnanlyzer" and "OutputModule".

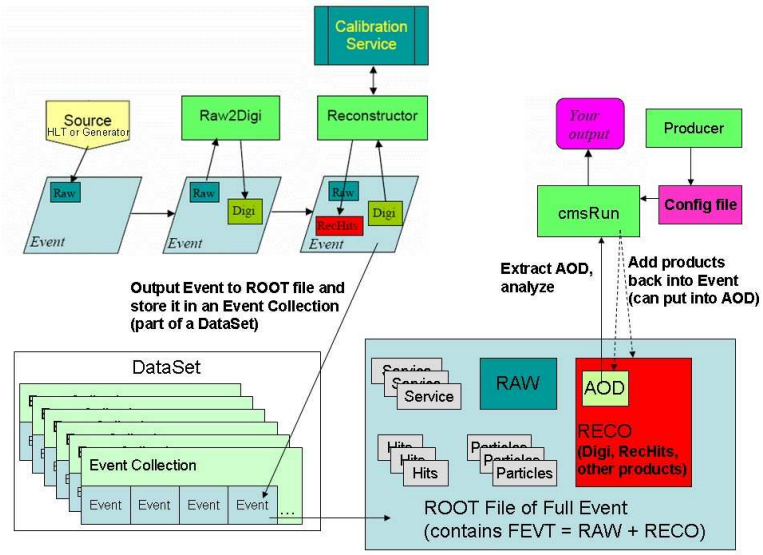

Figure 4.3: Framework[19]

- Source: This module reads event data from a root file or alternatively allows to generate events using PYTHIA. It is therefore more or less always needed.
- OutputModule: Allows to write output to external media.
- EDAnalyzer: An EDAnalyzer allows to study an event. It reads out the event's data and can write output, e.g. to a root-file. An EDAnalyzer was written to obtain the results presented in this report.

If one chooses to simulate the whole way, e.g. from event generation to reconstruction and analysis, the raw data provided by the GEANT simulation, simhits for the tracker, have to be treated further. In the digitization step the simhits are converted into "digis": This means that starting with the energy loss, the position and the direction stored in the Simhit of a passing particle the actual detector response is simulated (or better: parametrized using precompiled data tables). These digis are associated with a strip and store the "ADC"-information ("Analog to Digital Converter") that is the digital measure for the detector response.

Once the detector response has been simulated, the data obtained from the simulation and from the real experiment are treated in the same way. The signal from the detector is analysed and hits and tracks are reconstructed using the same algorithms for simulated and real data. Neighbouring hits are combined to clusters, when this group surpasses certain signal-to-noise ratios (cluster seed / neighbour strips / total cluster: TIB 4/3/5; TOB

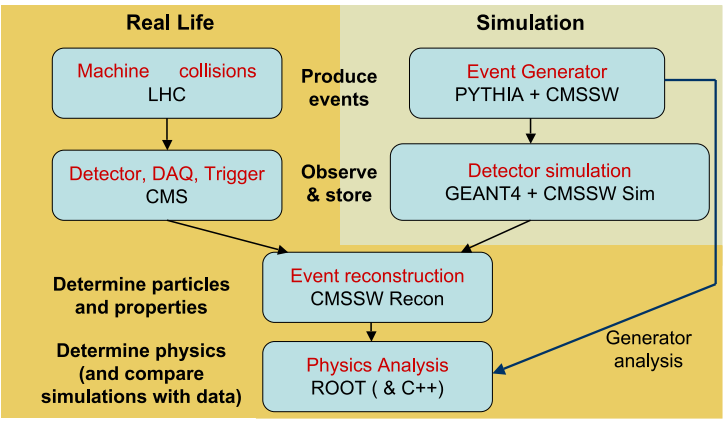

Figure 4.4: Comparison between data acquisition and handling in the simulation and the handling of data from the physical experiment[26]

5/2/5). These clusters are then interpreted as the actual signal from a particle passing through. The reconstructed hits/clusters and tracks then have to be analysed in order to reconstruct the physics processes that actually happened in the real experiment. The simulated data can be used to prepare analysis methods for the upcoming first measurements.

As mentioned above the algorithms that are used to reconstruct the events that happen in the real detector are validated and tested using the simulated data. In fig. 4.4 the data acquisition methods in the real experiment are opposed to the methods in the simulation. From the generation of collisions at the interaction point of the LHC until the Level 1 trigger decision the ways are separate: The Level 1 Trigger is designed in hardware to be fast enough for the very high bunch crossing frequency. The event reconstruction is carried out the same way and analysis prepared for the simulated and reconstructed data can be used for the data from the real experiment.

Chapter 5

Tracker Simulation - Results

In this chapter the results of the study of particles passing through the different barrel layers will be presented and the occupancy in the strip detector parts will be estimated. See 5.2 and 5.3 for details. To be able to obtain comparable data for particle type and hit distribution from all the different barrel layers an η- range of $|\eta| < 0.9$ has been chosen for specific analysis and discussion. The statistics of particles in this η- range is studied in section 5.1. The occupancy in section 5.3 is estimated for the full η-range. To keep the statistical errors at an acceptable level, the results were obtained from datasamples with 10000 events (p-p collisions), resulting in about $14 \cdot 10^6$ simhits in PXB1 - TOB6. The parameters of the PYTHIA event generation are shown in app A.

5.1 Generation of events - Statistics

In this section the statistics of the PYTHIA-generated events will be discussed. In fig. 5.2 the (semi) stable (status one - compare 4.2.2) particles with a flight direction into the $|\eta| < 0.9$ region are shown. For detailed tables compare the appendices B.1 and B.2.
As dominating results of the proton collisions we can mainly expect relatively light mesons as products of the combination of two quarks, hadrons from hadronization and some photons from primary interactions (compare

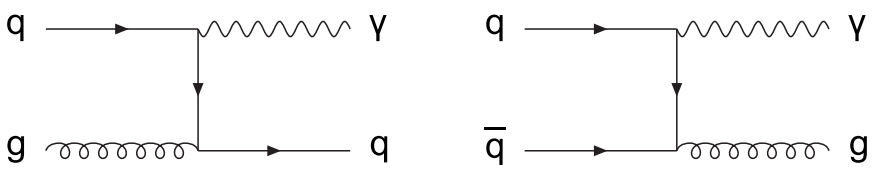

Figure 5.1: Direct photons can originate from quark-gluon Compton scattering (left Feynman diagram) and quark-antiquark annihilation (right). [27]

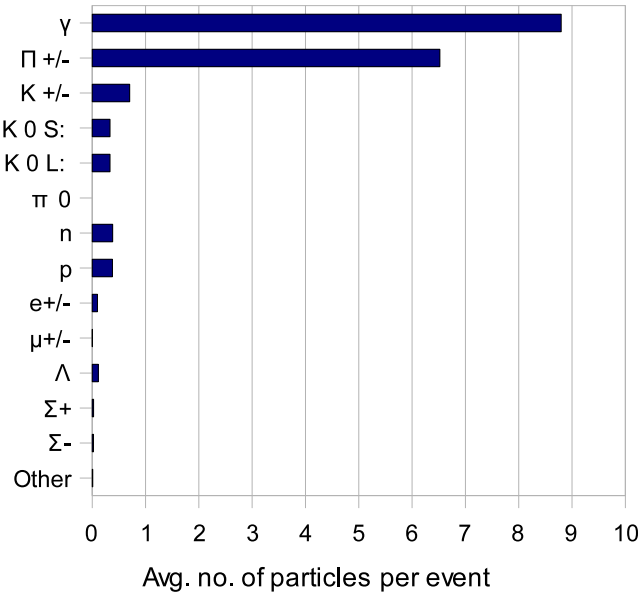

Figure 5.2: Particles with status one in $|\eta| < 0.9$ from PYTHIA event generation

fig. 5.1).
The most prominent products are photons and indeed light mesons: charged pions and K-mesons. The $\pi^0$is not found. Its mean life time of $\tau = (8.4 \pm 0.6) \cdot 10^{-17} s$ means that it decays after only 25.1 nm at a velocity of c. This almost immediate decay is handled within PYTHIA. We can see a large number of photons instead.
A considerable fraction of the electrons will probably originate from π^0as well: Only 0.56 % of all gen. particles in this range are electrons in comparison to 36.76 % charged pions. For every charged pion we expect 0.5 π^0. The second decay channel of the pion ($\pi^0 \rightarrow e^+e^-\gamma$with a probability of $1.198 \pm 0.032\%$) could explain up to 78 % of the primary electrons this way.
In addition to the mesons, electrons and photons there are protons, neutrons and strange baryons[1] originating from hadronization similar to the production of mesons. However, this process is suppressed as the production of baryons requires two $q\bar{q}$-pairs instead of only one for mesons.

[1]Baryon is the general term in particle physics for particles compound of three quarks. Protons and neutrons are the most familiar with a composition of uud (p) and udd (n).

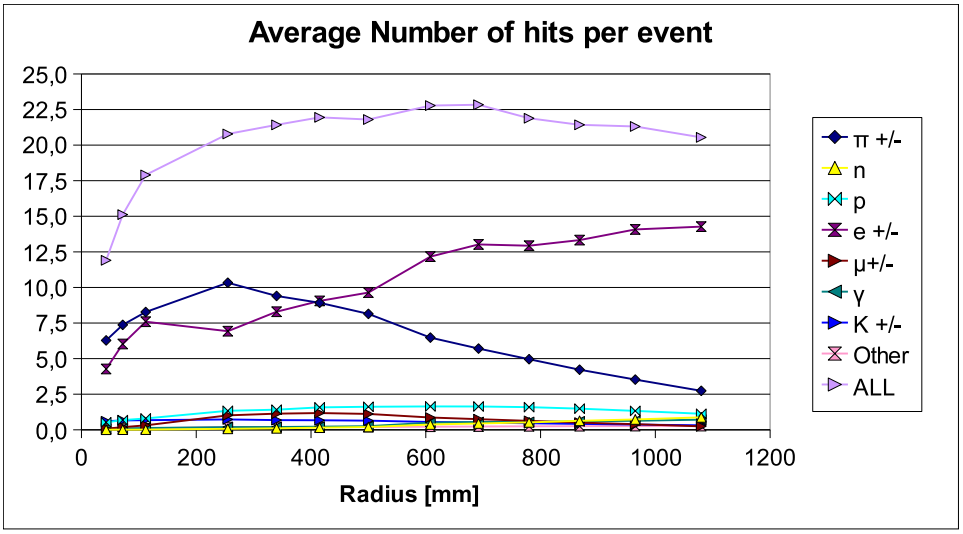

Figure 5.3: Statistics of particle types of the simhits in PXB, TIB and TOB, for a zoomed in picture compare 5.4

5.2 Simulation of the Tracker - Results

In this section the distribution of hits in the barrel regions for $|\eta| < 0.9$ of the tracker and the origin of the different particles causing hits in the tracker will be discussed. This η-selection includes the acceptance region of all the barrel tracker parts so that the results obtained for each layer are as comparable as possible. The layers with double-sided sensors have been treated as follows: The simhits were counted in total and then divided by two. Hereby the numbers for DS and SS layers should be comparable.

5.2.1 Statistics of Simhits in PXB, TIB and TOB

As discussed in section 4.2.3 the PYTHIA-generated events that have been discussed in section 5.1 are processed by GEANT to calculate simhits and simtracks. The number if simhits is illustrated in fig. 5.3 and the exact numbers including those from the generated events are given in tab. 5.1.
Clearly the most significant contributors to the hits are charged pions and electrons. Other charged particles cause hits as well, whereas neutral particles (except neutrons) and in particular photons do not leave a significant number of hits in the silicon sensors as they are much more sensitive to charged particles (compare 3.2.3).

Layer	**Radius [mm]**	$\pi^+/\ \pi^-$	n	p	e^+/e^-	$\mu^+/\ \mu^-$**:**
gen. Event	0	6.52	0.28	0.28	0.10	0.003
PXB 1	43	6.28	0.00	0.52	4.27	0.08
PXB 2	72	7.37	0.01	0.68	6.03	0.19
PXB 3	112	8.28	0.01	0.80	7.59	0.31
TIB 1	255	10.33	0.07	1.34	6.93	1.01
TIB 2	340	9.40	0.10	1.41	8.30	1.13
TIB 3	415	8.92	0.15	1.57	9.05	1.18
TIB 4	500	8.14	0.19	1.62	9.64	1.11
TOB 1	608	6.48	0.37	1.64	12.17	0.86
TOB 2	692	5.70	0.44	1.64	13.02	0.75
TOB 3	780	4.96	0.52	1.59	12.93	0.63
TOB 4	868	4.22	0.63	1.49	13.33	0.51
TOB 5	965	3.53	0.73	1.33	14.07	0.39
TOB 6	1080	2.74	0.87	1.13	14.27	0.24

Layer	**Radius [mm]**	γ	K^+/K^-	Other	All
gen. Event	0	8.79	0.70	0.83	17.72
PXB 1	43	0.07	0.60	0.06	11.90
PXB 2	72	0.09	0.66	0.08	15.12
PXB 3	112	0.13	0.67	0.10	17.90
TIB 1	255	0.19	0.73	0.19	20.78
TIB 2	340	0.20	0.68	0.20	21.42
TIB 3	415	0.22	0.67	0.19	21.95
TIB 4	500	0.25	0.64	0.19	21.80
TOB 1	608	0.50	0.55	0.21	22.78
TOB 2	692	0.55	0.51	0.23	22.84
TOB 3	780	0.55	0.46	0.24	21.89
TOB 4	868	0.59	0.41	0.25	21.42
TOB 5	965	0.63	0.37	0.26	21.31
TOB 6	1080	0.71	0.32	0.26	20.54

Table 5.1: Simhits in the barrel region of the CMS tracker

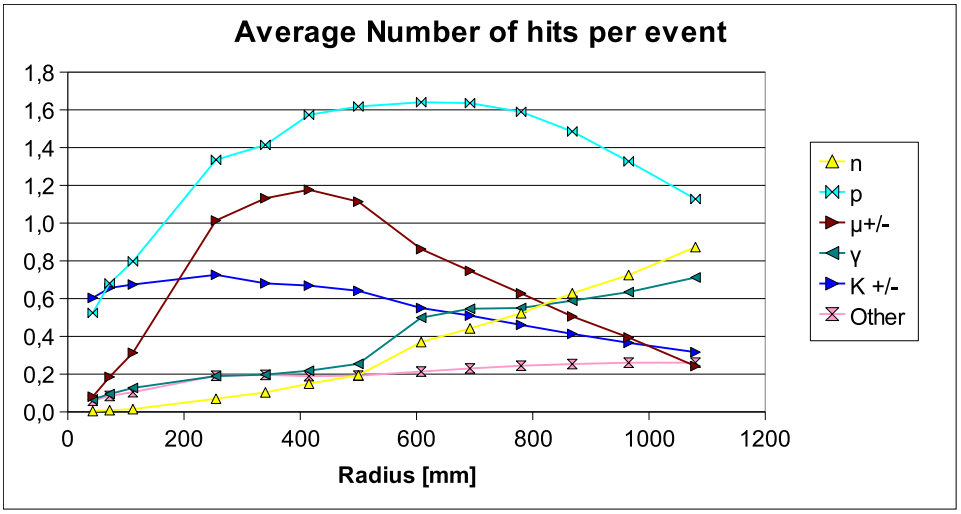

Figure 5.4: Additional zoomed chart of the statistics of particle types of the simhits in PXB, TIB and TOB

Transition: Generated events and hits in PXB 1

In contrast to the statistics we could obtain from the generated particles not all the particles cause a simhit, i.e. are detected in the tracker. This leads to some siginificantly different values at the time of the generation and the statistics obtained from the simhits that will be discussed here. We will go through the most important particle types step by step:

- Charged pions/kaons(6.52/0.70 to 6.28/0.60): The silicon sensors are very sensitive to charged mesons, the numbers are in good accordance.
- Photons(8.79 to 0.07): Although there is a significant number of photons in the examined η- direction, they do not appear in corresponding numbers in the statistics for the simhits. Only photons from low energy secondary processes interact strongly enough to leave a signal in the detector.
- Electrons(0.10 to 4.27): There are only a few primary electrons. However, there are a lot of simhits beginning from the very first layer. This is due to interactions with the tracker material - compare 5.2.4 for details.
- Muons(0.003 to 0.08): The muon hits originate almost exclusively from decays. Compare 5.2.5 for details.
- Protons and neutrons (0.28/0.28 to 0.52/0.00): The primary protons leave a signal in the detector, the neutrons do not leave a significant

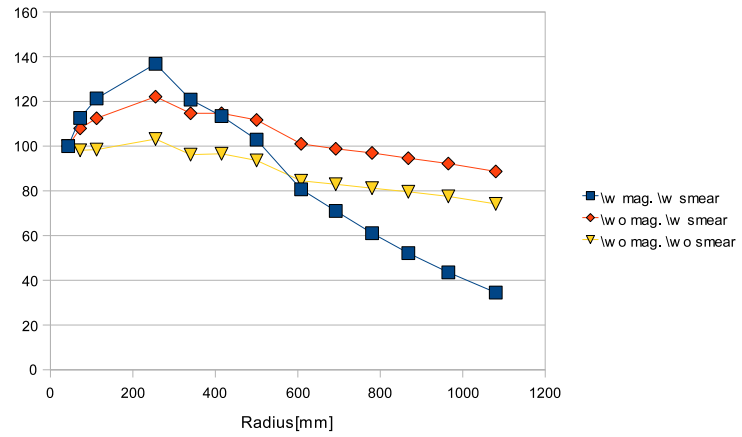

Figure 5.5: The normalized percentage (100% corresponds to the number of hits in PXB 1 seperately) of hits with the process type "Primary" for three different regimes: 1. With magnetic field and smearing (as in the experiment), 2. Without smearing, with magnetic field, 3. Without smearing and magnetic field. The absolute numbers are shown in app. C.1.

signal in comparison as they are uncharged.

- Other(0.83 to 0.06): The strange baryons and the K_S^0have a value of $c \cdot \tau$ of only several centimetres and are therefore largely decayed when reaching PXB 1. The K_L^0decays not quite that fast but it is neutral and not causing hits in the simulation.

Effects due to the global η-selection

The parts of the detector that contain simhits all have their own DetId (compare 4.2.3) associated with them. This DetId allows to access the global position. This global position is used to determine whether a hit lies within the $\eta <$ 0.9 cone or not. This global position is independent of the actual place of the interaction.
This η-selection leads to the effect that the number of hits from primary particles increases significantly in the first layers under the conditions that were chosen for the investigations in the following sections. For all the following investigations the smearing and the magnetic field are activated in the simulations as they would occur in the real experiment as well.
In fig. 5.5 the influence of the deactivation of the magnetic field and the smearing is shown. The smearing and the spiralling of particles can explain the increase of primary hits in the first layers:

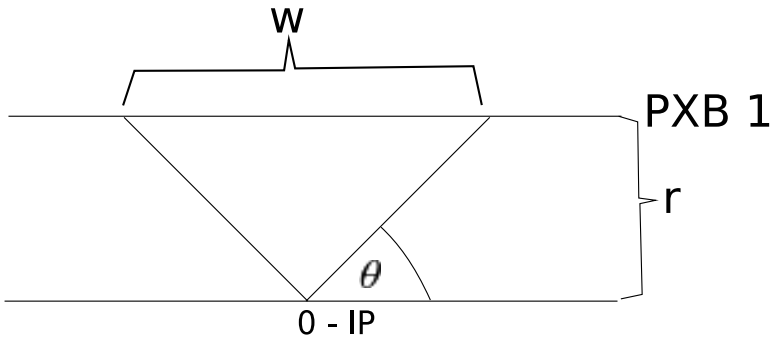

Figure 5.6: Illustration of the static η- cone

Spiralling particles due to the magnetic field Particles with low momenta spiral in the detector due to the 4T magnetic field superimposed by the solenoid (compare section 3.2). These particles can cause multiple hits before spiralling out of the acceptance region. Particles with a small ηcan cause more hits in "outer layers" (e.g. PXB 3 in comparison to PXB 1) than in the innermost layers as their acceptance region is larger. Deactivating the magnetic field in the simulation omits these spiralling particles. The increase without the magnetic field is much less significant.

Smeared interaction point In the innermost silicon detector layers we can observe a slight increase of primary hits of different particle types. This can partly be explained by the fact that the interaction point is smeared: The average bunch length of 7.6 cm leads to a distribution of the collision positions. In addition the bunches can cross at slightly different places, contributing to the smearing effect. Propagating the generated particles from these different starting points into the static $\eta<$ 0.9 cone leads to a considerable amount of particles entering the cone at a tranversally distant point.
$\eta=$ 0.9 corresponds to an angle of $\theta \cong 0.77 rad$. This means that the static cone covers a length of $w = \frac{2r}{\tan\theta} = 8.87 cm$ at the PXB 1 radius. This is of the order of the bunch length. Illustration: see fig. 5.6.
Deactivating the smearing and the magnetic field in the simulation leads to the disappearance of the increase of hits from primary particles as it appears in fig. 5.5 and C.2.

Trends from PXB to TOB

From PXB 1 to TOB 6 the composition of simhits changes considerably. The trends will be described here, more detailed explanations for pions, electrons, muons and protons will be given in the following subsections.
The number of hits in the selected η-cone increases in total to a maximum

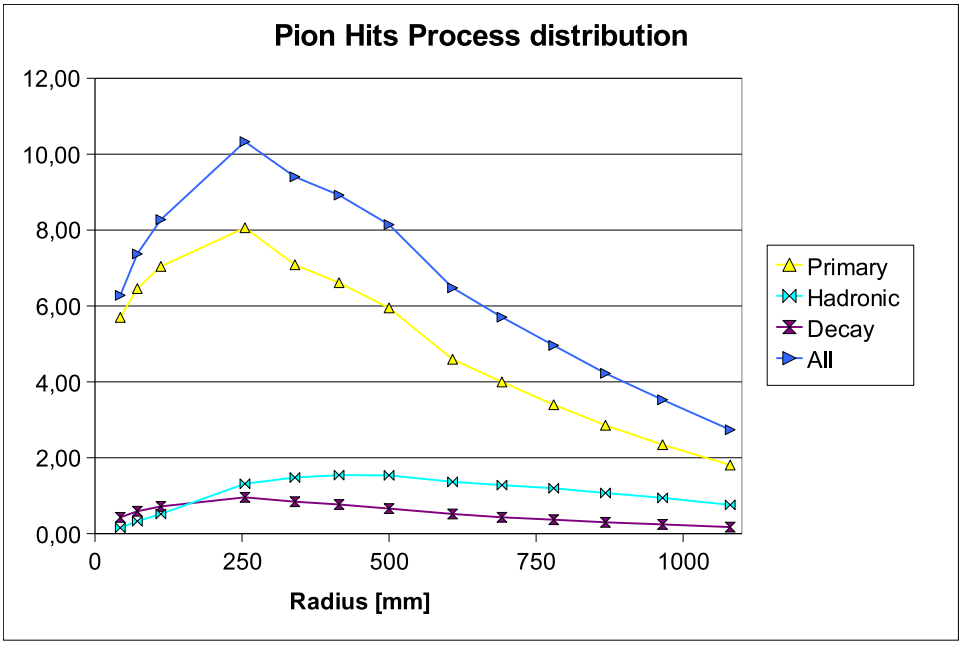

Figure 5.7: The chart shows the origin of pion hits in PXB, TIB and TOB according to the process type stored in the simhit-container, for a more detailed chart of lower-rate processes compare C.3.

of 22.84 hits in TOB 2 before decreasing again. The comparison to the 11.90 hits in PXB 1 yields an increase of 90%.
The dominant constituents of the simhits in the pixel and strip layers are electrons and charged pions. Other particles contribute to a much smaller extent. The average number of pion hits peaks in TOB 1 and decreases then. The number of electron hits is increasing over the full tracker region.
Only in the zoomed fig. 5.4 the other constituents can be distinguished. Proton hits and muon hits peak slightly delayed in comparison to the pion development and decreasein the outer layers. These particle types will be dicussed in more detail in the following sections.
Charged kaons are semistable particles just as the pions. Their number decreases continuously due to decays and probably spiralling. In the TOB-region there is a considerable amount of neutron hits. This increase originates at least partly from the backscattering of albedo neutrons emitted by the surrounding elecromagnetic calorimeters.[28]. Some low energy photon hits are observed as well, increasing in the outer layers.

5.2.2 Pion hit origin

In this subsection the origin of the pion hits will be discussed. Information from the simhit-datatype of CMSSW will be used here and in the following subsections. The process type stored for every simhit(compare 4.2.3) gives an indication of the origin of the particle that created the hit and is - for pion hits - displayed in fig. 5.7.
Main components of the hits are the primary prions produced in the QCD "minimum bias" interactions of the proton collisions. In addition there is an increasing part of pions from "hadronic processes" and decays. There are hadronic decay modes for charged kaons (21 % - $K^+ \rightarrow \pi^+\pi^0$), the K^0_S(70 % - $K^0_S \rightarrow \pi^+\pi^-$) and the strange baryons: The Λ is the most important of the strange baryons with its dominant decay mode (64 %) $\Lambda \rightarrow$ p π^-. There were 1.19 of these particles at the "gen. event"-stage and there is a maximum of 0.96 hits from "decays" in the TIB 1, so the decay hits can roughly be explained by this.
The "hadronic processes" are hard to subdivide, they include e.g. interactions of incident mesons and baryons with the nucleons in the tracker material. For "low energies" - in this context in accordance to the GEANT4 Physics Manual (pg.336) energies between 1 GeV and 25 GeV - the number of hadrons produced in hadron-nucleus collisions in the "Parametrization Driven Models" is given by eq. 5.1 (with atomic mass A, C(s) function of the centre of mass energy s and N_{ic}, the approximate number of hadrons generated in the initial collisions). The underlying concept is that incident particles collide with a nucleon inside the nucleus with Δ-baryons as intermediate states. Final states are the recoil nucleon, the scattered incident particle and after an eventual intra-nuclear cascade a number of secondary hadrons. The mean number of these secondary hadrons is given in the equation. The parameters used in this model are fitted to experimental data.

$$N_m = C(s)A^{\frac{1}{3}}N_{ic} \tag{5.1}$$

5.2.3 Proton hit origin

The number of proton hits increases rapidly from inner to outer layers, peaks in TOB 1 with 1.64 hits and goes down to 1.13 hits in TOB 6.
In the $|\eta| < 0.9$ range there are 0.28 protons from the PYTHIA generated events stage. These primary protons leave a clear signature in the detector with 0.32 hits in PXB 1 decreasing to 0.20 hits in TOB 6.
There are up to 0.10 hits (TIB 1 - 4) originating from decays. From the PYTHIA event generation there is a number of strange baryons, namely the $\Sigma^+(0.03,\ c\tau = 2.4cm)$, the $\Sigma^-(0.02,\ c\tau = 4.4cm)$ and the $\Lambda(0.11,\ c\tau = 7.9cm)$. These unstable strange baryons decay quickly and the main decay modes of the $\Lambda$and the Σ^+involve proton production:

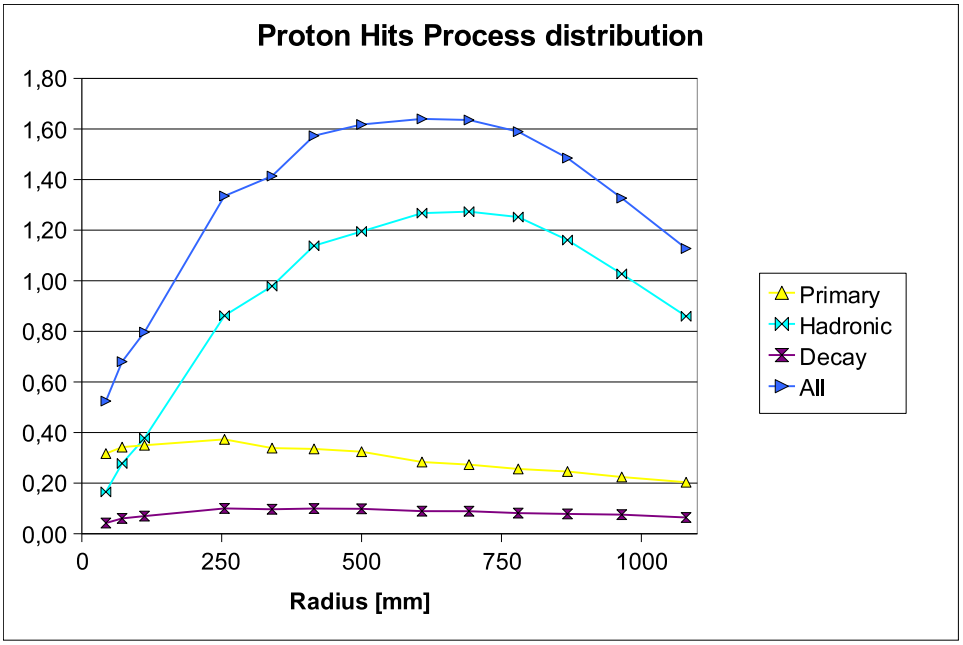

Figure 5.8: The chart shows the origin of proton hits in PXB, TIB and TOB according to the process type stored in the simhit-container, for a more detailed chart of lower-rate processes compare C.4.

- Λ: 63.9% $\Lambda \rightarrow p\pi^-$
- Σ^+: 51.6% $\Sigma^+ \rightarrow p\pi^0$

These two decay modes add up to 0.086 protons alone, so they are thought to be the main component of the protons from decays.
The process type "hadronic" is responsible for most of the hits in this η-region. Comparing the trends in fig. 5.8 and the one for pions (fig. 5.7) shows that the number of hits peaks with a "delay", but is similarly shaped. Hadronic interactions like pion-nucleon collisions result in the creation of protons as well and the high number of pion hits in the inner strip layers results in the production of a lot of protons that hit the detector in the subsequent layers.

5.2.4 Electron hit origin

There is a wide variety of processes causing electron hits, but pair production, Compton scattering and delta-rays are the most important in terms of the number of hits. Electrons from delta rays make up most of the hits in the pixel detector, electrons originating from photon conversion are getting more and more important in the strip detector, in the outermost layers electrons

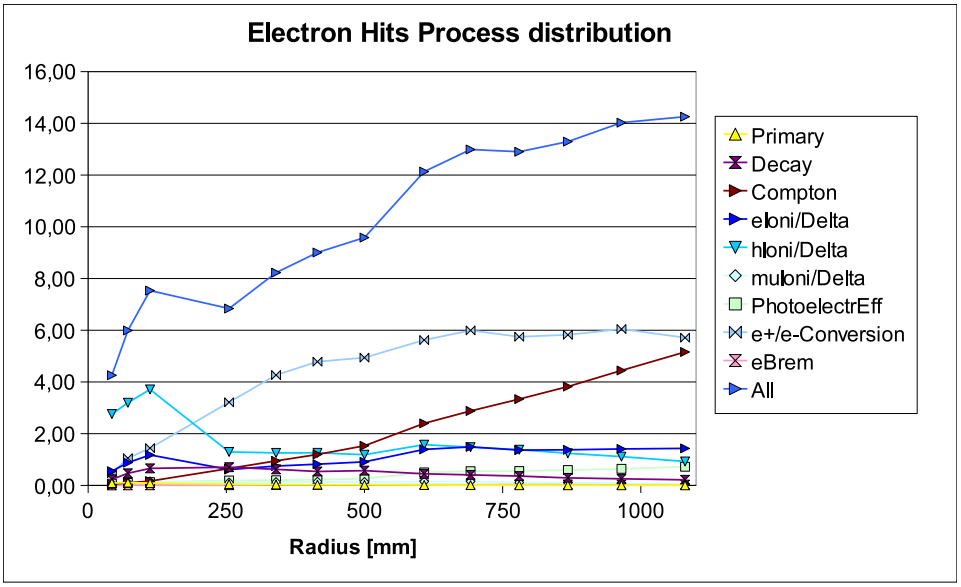

Figure 5.9: The chart shows the origin of electron hits in PXB, TIB and TOB according to the process type stored in the simhit-container, for a more detailed chart of lower-rate processes compare C.5.

originating from Compton scattering become almost as dominating. These processes will be covered seperately, other processes play a minor role, but contribute to the hits as well and should at least be mentioned: The photo-electric effect (absorption of photons and emission of electrons) and decays (e.g. from K^+/K^-).

Delta rays

Delta- or δ-rays are made up of electrons that originate from ionization caused by charged particles. However, not all electrons originating from ionization form a δ-ray. These electrons are called δ-rays, when their energy is sufficiently high to create secondary ionizations. The threshold for the simulation of δ-rays in GEANT4 is always 1 keV or larger. Cross sections for the Möller scattering of electrons and the Bhabha scattering of positrons are given in section 8.1, the cross section for ionization by hadrons and ions is given in section 9.1 of the GEANT Physics reference manual. [22]
These electrons are the most important constituent of the electron hits in the pixel detector. Due to the proximity of the pixel layers the delta-rays can leave hits in the surrounding layers although their energy is comparatively low to the primary particles. According to the incident particle they are denoted as hIoni/Delta or eIoni/Delta in fig. 5.9. In the outer layers the importance of δ-rays is overtaken by the increasing number of electrons from photon conversion and Compton scattering.

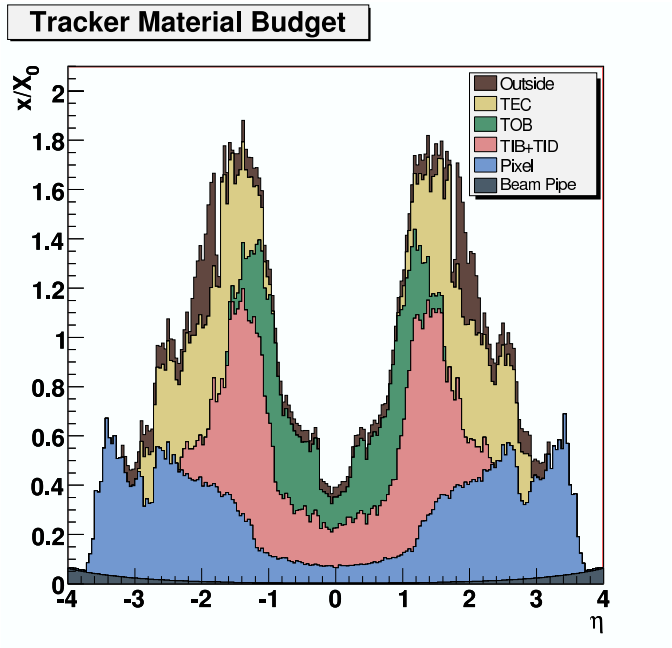

Figure 5.10: Material Budget

Photon conversion

Just as the annihilation of a electron/positron pair results in the production of a photon, a photon with a sufficiently high energy (i.e. more than twice the rest energy of apositron/electron - 1.022 MeV) can convert into an electron/positron pair. As momentum has to be conserved, a third body - usually a nucleus - has to be involved. The mean free path of a photon for pair production, which is explicitly given in eq. 5.2 (as in [18]), is linked to the radiation length as $\lambda \cong \frac{9}{7} X_0$. The tracker material budget in terms of the radiation length X_0 is given in fig. 5.10.

$$\frac{1}{\lambda_{pair}} \cong \frac{7}{9} 4Z(Z+1)Nr_e^2\alpha \left[\ln(183Z^{-\frac{1}{3}}) - f(Z)\right] \qquad (5.2)$$

with Z: atomic number, N: density of atoms, $\alpha = \frac{1}{137}$,

f(Z): Couloumb correction, $r_e = \frac{e^2}{mc^2}$ - classical electron radius

Not all photon interactions with matter above $E_{photon} = 1.022MeV$ result in the production of an e^+/e^--pair. Before the photon energy exceeds several tens of MeV Compton scattering is the dominant process. The probability

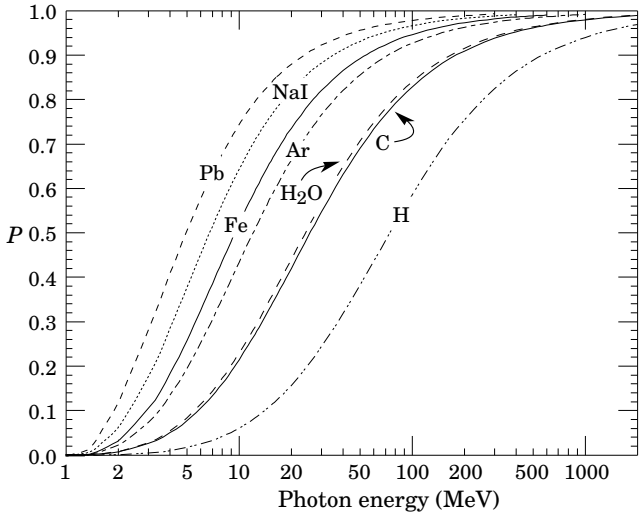

Figure 5.11: Probability P that a photon interaction will result in conversion to an e^+/e^--pair [4]

P of conversion in different materials is given in fig. 5.11. Together with the mean free path we obtain the expression in eq. 5.3 for the conversion of photons.

$$P_{conv} = P\left[1 - e^{-\frac{x}{\lambda}}\right] \tag{5.3}$$

with the thickness x of the absorber

For a rough estimation we assume from fig. 5.10 an average radiation length of 0.1 for the pixel detector (i.e.$\lambda \cong 0.13$) and P=1 for photons above 0.1 GeV. This would yield about 0.95 more electrons/positrons which corresponds to the hits in PXB 3. For more detailed calculations the momentum distribution of the photons and the spiralling of the created low-energy electrons due to the magnetic field would have to be taken into account.
The material in the strip detector increases the amount of electrons from conversions further, but as low-momentum electrons are bend away and do not propagate into the outermost regions the hits from conversions do not keep increasing in outer layers.

Compton scattering

Compton scattering describes the decrease in energy of high energy photons (x-ray and above, lower energy range than in photon conversion) when they interact with free electrons. When the energy of the incident photon is high in comparison to the binding energy of electrons in the shell of atoms, these electrons can be treated as if free as well. The electrons the incident photons

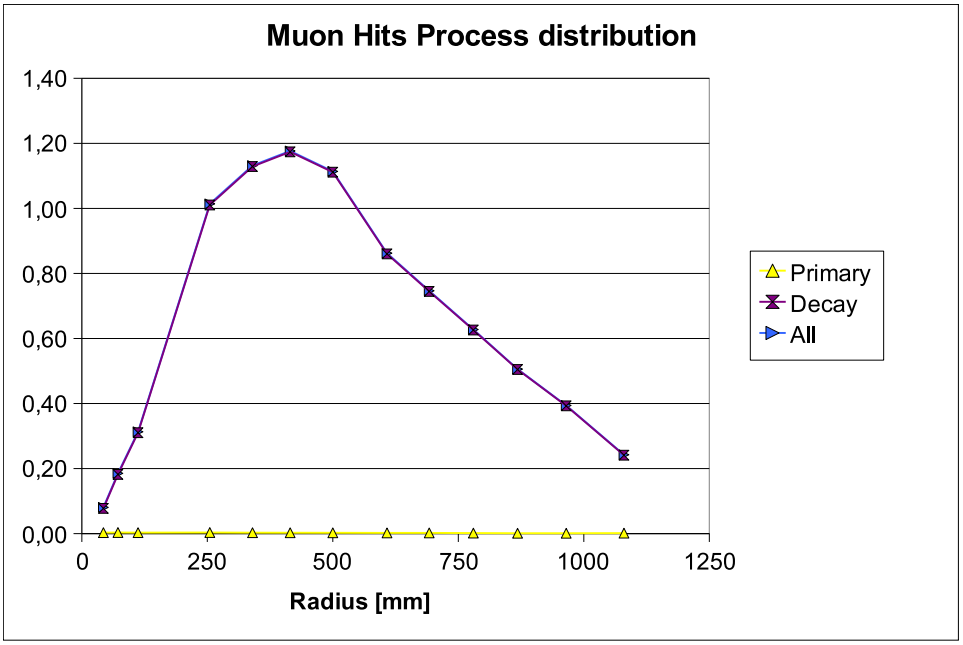

Figure 5.12: The chart shows the origin of muon hits in PXB, TIB and TOB according to the process type stored in the simhit-container.

hit are recoiled and can propagate through the detector leaving htis, when the energy transfer was high enough.
It does not neccessarily mean that the number of photons decreases significantly, when the number of electron hits from photon conversion does not increase further in outer layers. As it can be seen in fig. 5.8 the number of electron hits from Compton scattering increases. Compton scattering is the dominating process for photon energies below the range where photon conversion becomes dominant (compare fig.5.11) and as there are additional photons being produced in the tracker, e.g. by electrons loosing energy by bremsstrahlung, the number of Compton scattering processes can keep on increasing - even in outer layers.

5.2.5 Muon hit origin

The muon hits originate almost exclusively from decays as shown in fig. 5.12. The number of primary muons and therefore the number of hits from these is almost negligible (0.0033 in TIB 1, decreasing to 0.0014 in TOB 6). The main decay modes of charged pions and kaons are into muons:

- π^+/π^-: 99.9% - $\pi \rightarrow \mu + \bar{\nu_\mu}$
- K^+/K^-: 63.44% - $K \rightarrow \mu + \bar{\nu_\mu}$

Due to the high number of charged pions, they will be the dominant source for muons. As their number decreases significantly in the strip layers, the number of muons decreases similarly, but with a delay: The number of muon hits peaks in TIB 3, the number of pion hits peaks in TIB 1.

Pion decay

The decay of pions and kaons produces mainly muons instead of electrons. The electronic decay is strongly supressed. This is due to the conservation of the angular momentum and the different masses of muons and electrons. In the rest frame of the pion the total angular momentum is nought. When the pion decays the muon/electron and the antineutrino leave into adjacent directions. They cannot carry any orbital angular momentum because of the short-range weak force. To conserve the total angular momentum the helicity of the muon/electron has to be $+\frac{1}{2}$ as well, because the spin of the antineutrino is parallel to its flight direction. The probability to find the muon/electron in this state is in the weak force proportional to $\left(1-\frac{v}{c}\right)$ and as the muon is much more massive than the electron this factor is much smaller for electrons.
This circumstance finds expression in the matrix element as well which is shown for the electron in eq. 5.4. The expression for muons is analog, so we can obtain the ratio of the decay rates after integrating over $d\Omega$ to $1.28 \cdot 10^{-4}$ as shown in eq. 5.5. For an even more detailed discussion compare Peter Schmüser's book[29].

$$|\mathcal{M}|^2 = 4G_f^2 f_\pi^2 m_\pi^2 p(E-p) = G_f^2 f_\pi^2 m_\pi^2 m_e^2 (m_\pi^2 - m_e^2)) \tag{5.4}$$

$$\frac{\Gamma(\pi^- \to e^- + \bar{\nu_e})}{\Gamma(\pi^- \to \mu^- + \bar{\nu_\mu})} = \frac{m_e^2(m_\pi^2 - m_e^2)^2}{m_\mu^2(m_\pi^2 - m_\mu^2)} = 1.28 \cdot 10^{-4} \tag{5.5}$$

5.3 Strip Detector Occupancy

In this section we will estimate the occupancy in the barrel layers (TIB and TOB) of the silicon strip detector. The occupancy for the pixel layers can be determined in a similar way, but the extraction of numbers from the simulation is slightly different. Due to the higher number of channels we would expect a lower occupancy, but there was not enough time to get these numbers as well.
The occupancy for the strip detector will be used in two different forms: The strip occupancy is the ratio of the number of affected and the number of all strips[2] for each layer; the simhit occupancy relates the number of simhits in

[2]The number of all strips, i.e. the number of channels, was calculated from the given number of APVs just as shown in tab. 3.2.

each layer with the total number of strips. The occupancy has to be kept low in order to allow a reliable hit and track reconstruction. The first step will be a rough "paper-calculation" with results that we need in order to get exact values for the occupancy from the simulation, then.
In the previous section we tried to explain the origin of hits in the barrel layers and give explanations for the developments we can observe. This is important in order to be able to understand and interpret other results from the simulations - and later the actual experiment. We started with the PYTHIA-generated events and examined what happened to the particles when they propagated through the detector. The simulation was useful to provide helpful information, e.g. the process type information. E.g. we saw that the number of hits in the examined η-range increases from 11.90 hits in PXB 1 to up to 22.84 hits in TOB 2. And all this from starting with "only" 7.76 charged particles into this direction. The simulation includes decays and in-depth models for interactions with matter. If we neglect these and work with the data obtained from the gen. event stage, we can perform the following calculation:

5.3.1 Paper calculation

In the simulation data that have been analysed, the cross section for the minimum bias interactions is $\sigma = 79.19mb$. The peak luminosity of the design LHC is $\mathcal{L} = 10^{34}cm^{-2}s^{-1}$. Taking into account the empty bunches (mentioned in section 2.2.2) as $f_{bunch} = \frac{3564}{2808} \cong 1.27$ and integrating over 25 ns (corresponding to the 40 MHz bunch crossing frequency) we obtain the average number of minimum bias events as

$$N_{events} = f_{bunch}\,\sigma \int \mathcal{L}\,dt = 25.13$$

This number will be used for the occupancy numbers from the simulation as well.
There are numerous assumptions for the charged particle density distribution at the LHC. For the plateau $|\eta| < 2.5$ we assume the comparatively low value of $\frac{dN_{ch}}{d\eta} \cong 4.0$ in order to be consistent with the PYTHIA data as shown in fig. 4.1. However, there is a significant uncertainty in the predictions here: The previously cited "Prediction for minimum bias and the underlying event at LHC energies" [15] suggests a value of $\cong 7.0$ for PYTHIA 6.214 "tuned" and $\cong 5.5$ for the event generation with PHOJET 1.12, a talk by Ferenc Siklèr at the CMS Tracker Days (11 March 2008) suggests $\frac{dN_{ch}}{d\eta} \cong 4.4$. Minimum bias data will be the first physics results when the LHC starts running at low luminosity. Only then this question will be answered definitely.
Assuming the charged particle density from the used dataset, we obtain the number of tracks of charged particles for a desired η-range as $N_{tracks} \cong$

$(2\eta_{max})\frac{dN_{ch}}{d\eta}N_{events}$. A hit in the strip layers affects on average more than one strip. Some of the deposited charge diffuses to neighbouring strips, leading to a cluster size of about $\alpha = 3$ strips. We will assume that the tracks propagate straight through the detector and leave three strips affected per layer.
We can obtain an estimation for the number of hits in a certain layer (with its specific coverage range $\Delta\eta$) as

$$hits = \Delta\eta \, \frac{dN_{ch}}{d\eta} \, N_{events}\alpha$$

The occupancy can then be calculated for the double-sided TIB layers 1 and 2 as

$$Occ = \frac{hits}{\frac{1}{2}no.of strips}$$

This yields the following results:
For the TIB 1 ($\Delta\eta = 3.6$, strips: 516096): $Occ \cong \frac{1085.6}{258048} = 0.42\%$
For the TIB 2 ($\Delta\eta = 3.1$, strips: 663552): $Occ \cong \frac{934.8}{331776} = 0.28\%$
Important parameters for this hand calculation - that should roughly scale with the real occupancy - are the number of events per bunch crossing and the charged particle density distribution $\frac{dN_{charged}}{d\eta}$. To get a more realistic picture of the occupancy during high luminosity LHC operation the signal event that will always be superimposed for the ≈ 100 permanently saved events would have to be taken into account. In the following section the occupancy results from the simulation will be discussed. Starting point is the same cross section and charged multiplicity distribution as this was taken from the simulation for this calculation.

5.3.2 Occupancy results(simhits and clusters)

In sections 4.2.3 and 4.2.4 the datatypes of simhits and clusters were explained. From the simhits and the clusters an occupancy can now be calculated. The "SiStripCluster" class from CMSSW contains a vector with the signal amplitudes of the clusterized strips. The size of this vector is equivalent to the cluster size α that was used in 5.3.1 in order to estimate the relation between hits and the number of affected strips.
The "simhit occupancy" is the ratio of the no. of simhits in the examined layer and the total number of strips. The "strip occupancy" is the ratio of the number of affected strips, i.e. the added up size of clusters in each layer, and the total number of strips in each layer. The results are calculated with an average number of events of $N_{events} = 25.13$, i.e. the number of simhits/clusters obtained for one minimum bias interaction as obtained from the simulation is multiplied with this value. The occupancies are shown in fig. 5.13 and the precise numbers are given in tab. 5.2.

The results show a continous decrease in the occupancy from inner to

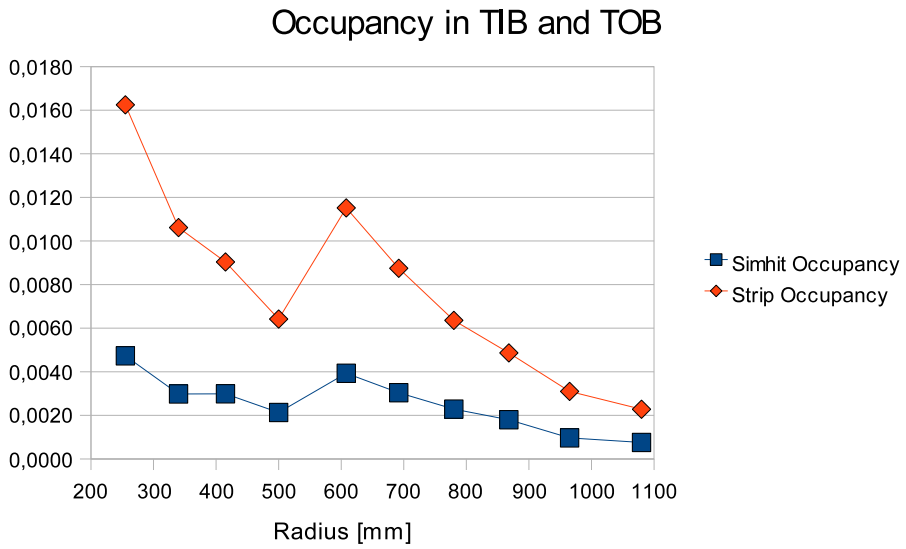

Figure 5.13: The occupancy is shown as ratio of 1. $\frac{\text{no. of simhits}}{\text{no. of strips}}$ and 2. $\frac{\text{no. of affected strips}}{\text{no. of strips}}$

Layer	Strips	Radius [mm]	Simhit Occupancy	Strip Occupancy	Difference to CMS-Note
TIB 1	516096	255	$4.73 \cdot 10^{-3}$	$16.2 \cdot 10^{-3}$	1.72
TIB 2	663552	340	$2.98 \cdot 10^{-3}$	$10.6 \cdot 10^{-3}$	1.70
TIB 3	276480	415	$2.99 \cdot 10^{-3}$	$9.04 \cdot 10^{-3}$	1.88
TIB 4	331776	500	$2.13 \cdot 10^{-3}$	$6.42 \cdot 10^{-3}$	2.03
TOB 1	516096	608	$3.93 \cdot 10^{-3}$	$11.5 \cdot 10^{-3}$	1.65
TOB 2	589824	692	$3.04 \cdot 10^{-3}$	$8.75 \cdot 10^{-3}$	1.60
TOB 3	331776	780	$2.29 \cdot 10^{-3}$	$6.36 \cdot 10^{-3}$	1.73
TOB 4	368640	868	$1.80 \cdot 10^{-3}$	$4.86 \cdot 10^{-3}$	1.64
TOB 5	608256	965	$0.97 \cdot 10^{-3}$	$3.09 \cdot 10^{-3}$	1.61
TOB 6	681984	1080	$0.76 \cdot 10^{-3}$	$2.28 \cdot 10^{-3}$	2.63

Table 5.2: Occupancy in the silicon strip barrels

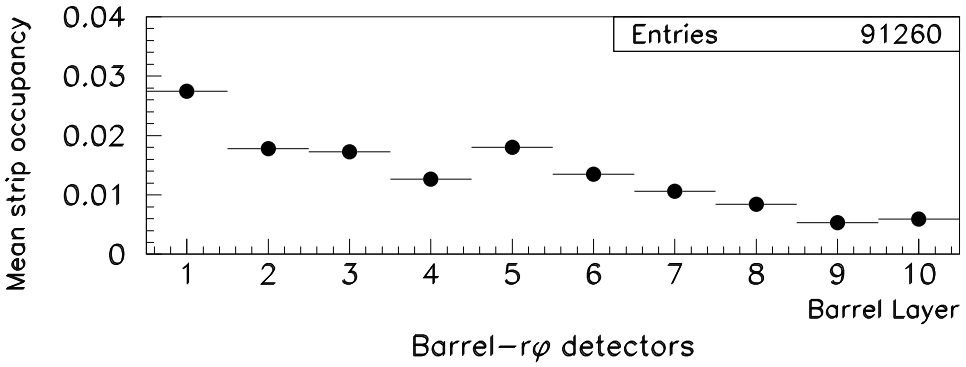

Figure 5.14: Strip occupancy dependence on barrel layers from the CMS Note 2002/047: Barrel Layer 1-4 = TIB 1-4; BarrelLayer 5-10 =TOB 1-6 [16]

outer layers. The step from TIB 4 to TOB 1 can be explained by the different strip size (discussed in section 3.2.2) in the TOB, leading to fewer strips in comparison to the covered area than in the TIB. TIB 4 is a SS layer with 331776 strips, TOB 1 is a DS layer with 516096 strips (equivalent to ≈ 258048 as a SS layer) as shown in tab. 5.2. The average simhit occupancy is 0.26 %, the average strip occupancy from the simulations is 0.79 %. This corresponds to an average cluster size of $\alpha = 3.05$.

Comparison to previous results

In the CMS Note 2002/047 [16] the expected data rates from the silicon strip tracker were discussed. The occupancy due to minimum bias events was therefore estimated. Results for the occupancy are shown in fig. 5.14. There is a discrepancy to the obtained results. This discrepancy is given as a factor in tab. 5.2. As the roughly constant factor[3] suggests there are some systematic differences that cause the different level of occupancy:

- In the CMS Note the parameters used for the PYTHIA event generation generated minimum bias events with a cross section of 101 mb in contrast to the minimum bias event cross section of 79.19 mb that is given by the PYTHIA parameters (those used for the validation of new CMSSW-versions, compare appendix A) that were used now. The

[3]The step in the outermost layer - TIB 6 - is probably due to a "bug in the Monte Carlo production" used in the simulation for the CMS-Note: Low momentum photons from the ECAL were producing (too many) hits in the tracker, especially the endcaps. Although the background in the barrel layers is not that high, this could be the reason for the suddenly higher discrepancy in TOB 6 as well. [17]

number of superimposed minimum bias events in the CMS Note is with 32 events therefore 28% higher as 25.13 which was used for our results.

- The CMS Note takes into account one signal event. For the high luminosity case this is said to increase the occupancy by about 12 %, i.e. 0.0018 for the mean occupancy of 0.017. There is no signal event included in the analyzed data set here. Adding the given signal event occupancy to the results would give 0.0097 instead of 0.0079 now - 23 % more.

- The charged particle density distribution is not explicitly mentioned in the CMS Note, but as dicussed before, $\frac{dN_{ch}}{d\eta} \cong 4.0$ as in the here used dataset, is on the lower end of the estimations mentioned in section 5.3.1 - e.g. 7.0 and 5.5 from the minimum bias prediction paper [15]. Assuming 5.5 for $\frac{dN_{ch}}{d\eta}$ in the plateau region would mean 37.5% more primary tracks from charged particles.

A final answer to the best choice of parameters can only be given by the experiment itself as the extrapolation of previous experimental results leaves space for uncertainties. Measurements from the Tevatron with its centre of mass energy of 1.96 TeV as the predeccessor can not guarantee an accurate prediction for the LHC with its centre of mass energy of 14 TeV.
Combining the above mentioned uncertainties and different considerations can explain the difference between the CMS Note and the current results. However, the simulations can only be rectified or falsified by the actual operation of the LHC. Results obtained from the LHC will then allow to extend the models in the simulation to even higher energy scales.

Chapter 6

Conclusions

The design of large-scale experiments with significantly higher complexity in comparison to the predecessor is always a difficult task. Thanks to the progress in information technology simulations can help in the design of new particle physics experiments like those at the LHC.

In the interplay of simulations and physics motivated thoughts the results for the occupancy from the simulation can be interpreted and we were able to explain the general trends in the constitution of hits in the tracker barrel layers. Hits from electrons and charged pions are the main contributors to the occupancy in the silicon strip tracker.
Although the absolute value for the mean occupancy in the barrel layers of $\approx 1.39\%$ might turn out as lower than the actual physical value at the experiment, the attempted explanations for the general trends should remain valid. It would probably be useful to perform further studies on the occupancy with other tunings of PYTHIA than those used for the CMSSW-release validation as well, e.g. those from the Min-Bias paper [15]. The $\frac{dN_{ch}}{d\eta}$ charged particle density distribution and the predicted cross sections are important parameters for the absolute occupancy values and should therefore be as near to the most recent findings as possible.

When the results from the first months of CMS-running are incorporated into the simulation, the design of a new tracker for the SLHC will become easier. The considerably increased luminosity will require a tracking system with an even higher resolution that has to withstand even harsher radiation conditions. An understanding of the current tracker will help to estimate the required design priorities for the to-be-developed tracking system of CMS in SLHC conditions and the enhanced simulations will allow to narrow the best proposals down.

Acknowledgements

I would like to thank all those who helped me with the project. Andrew Rose helped me getting started with CMSSW and told me about the stacked pixel detector proposal for the SLHC. Mark Pesaresi supported me when physics and simulations were working out – and when they were not working out, encouraging me to go on. It was nice to get to know Konstantinos Petridis, who was open to my questions at any time. And, of course, many thanks to Geoffrey Hall for making the project possible, guiding me through the time and providing support when needed.

Bibliography

[1] **LHC Design Report, v 1; The LHC Main Ring**
cernrep / 2004-003-v1

[2] **Website run by the DPG**
http://www.weltderphysik.de/de/182.php

[3] **Physics at LHC, John Ellis**
CERN-PH-TH/2006-239, http://arxiv.org/pdf/hep-ph/0611237v1

[4] **Review of Particle Physics**
W.-M. Yao et al. (Particle Data Group), J. Phys. G 33, 1 (2006) and 2007 partial update for edition 2008 (URL: http://pdg.lbl.gov)

[5] **LHC and its preaccelerators**
http://en.wikipedia.org/wiki/Image:LHC.svg

[6] **ATLAS Technical Design Report Volume 1**
ATLAS TDR 14, CERN/LHCC-99-14

[7] **CMS - Expression of interest in the SLHC**
CERN/LHCC 2007-014, LHCC-G-131, 15 March 2007

[8] **CMS Physics TDR: Volume I (PTDR1), Detector Performace and Software**
CERN-LHCC-2006-001, 2 February 2006

[9] **The CMS experiment at the CERN LHC, Article for the Journal of Instrumentation**
http://cmsdoc.cern.ch/cms/Publications/detpaper/CMS-JINST.pdf, 6 January 2008

[10] **CMS ECAL Technical Design Report**
CERN/LHCC 97-33, 15 December 1997

[11] **Inaugural Lecture Tejinder S. Virdee**
Imperial College, 14 October 1998

[12] **CMS document for guides**
cmsinfo.cern.ch/outreach/CMSdocuments/ForGuides/CMSdocumentforGuides.pdf, Dave Barney, 27 November 2003

[13] **Sensor design for the CMS Silicon Strip Tracker**
L. Borrello, A. Messineo, E. Focardi, and A. Macchiolo, CMS Note 2003-020, 2002

[14] **Development and Evaluation of Test Stations for the Quality Assurance of the Silicon Micro-Strip Detector Modules for the CMS Experiment**
Michael Pöttgens, urn:nbn:de:hbz:82-opus-22195, 11 March 2008

[15] **Prediction for Minimum Bias and the Underlying Event at LHC Energies**
A.Moraes,C.Buttar,I.Dawson:DOI10.1140/epjc/s10052-007-0239-1,16February2007

[16] **Expected Data Rats from the Silicon Strip Tracker**
CMS Note 2002/047, 27 November 2002

[17] **Updates to the data rates quoted in CMS Note 2002/047**
http://cms-btau-datahandling.web.cern.ch/cms-btau-datahandling/SiStripDataRates04.html, December 2004

[18] **Techniques for Nuclear and Particle Physics Experiments**
W.R. Leo, Springer Verlag Berlin, 1994

[19] **"CMSSW Application Framework" article in the TWIKI**
https://twiki.cern.ch/twiki/bin/view/CMS/WorkBookCMSSWFramework

[20] **PYTHIA 6.4 - Physics and Manual**
hep-ph/0603175, March 2006

[21] **GEANT4 Collaboration Homepage**
http://geant4.web.cern.ch/geant4/

[22] **GEANT4 9.1 Physics Reference Manual**
http://geant4.web.cern.ch/geant4/UserDocumentation/UsersGuides/PhysicsReferenceManual/fo/PhysicsReferenceManual.pdf, 14 December 2007

[23] **Minimum bias interactions and the underlying event**
http://www.shef.ac.uk/physics/research/hep/atlas/ukphys/meeting8/slides/moraes.pdf, A. Moraes, ATLAS - UK Physics Meeting, September 2002

[24] **WS 2007/2008 - Physik am LHC**
http://www-eep.physik.hu-berlin.de/lectures/hadcol/WS0708_lhc_lecture_kap1.pdf, *Martin zur Nedden, HU Berlin*

[25] **Introduction to elementary particles**
David Griffiths, 1987 John Wiley and Sons, Inc.

[26] **Simulation Basics in CMS**
http://docdb.fnal.gov/LPC/DocDB/0000/000038/003/AllUSCMS2006-May26.pdf , *H.W.K. Cheung, May 2006*

[27] **Direct Photon Measurement in Proton-Proton and Deuteron-Gold Collisions**
http://igitur-archive.library.uu.nl/dissertations/2008-0417-200620/russcher.pdf , *Universiteit Utrecht, M. J. Russcher, April 2008*

[28] **Performance of the CMS tracker in high level trigger**
doi:10.1016/j.nima.2003.08.103, CERN EP Division, M. Lenzi, September 2003

[29] **Feynman - Graphen und Eichtheorien für Experimentalphysiker**
ISBN 978-3540584865, Peter Schmüser, Springer Verlag, 2nd edition, October 2007

Appendix A

PYTHIA parameters for min-bias events

The following config-file has been used to generate events for the validation of new CMSSW-versions and is available from:

http://cmssw.cvs.cern.ch/cgi-bin/cmssw.cgi/CMSSW/Configuration/ReleaseValidation/data/MinBias.cfg?revision=1.8&view=markup&pathrev=CMSSW_1_7_7

```
process Rec =
{
  untracked PSet maxEvents = {untracked int32 input = 1}

  untracked PSet ReleaseValidation =
  {
    untracked uint32 totalNumberOfEvents = 5000
    untracked uint32 eventsPerJob        = 250
    untracked string primaryDatasetName  = 'RelValMinBias'
  }
  untracked PSet configurationMetadata =
  {
    untracked string version = "$Revision: 1.8 $"
    untracked string name = "$Source: /local/projects/CMSSW/rep/CMSSW/
    Configuration/ReleaseValidation/data/MinBias.cfg,v $"
    untracked string annotation = "RelVal MinBias"
  }

  include "Configuration/ReleaseValidation/data/Services.cff"
  include "Configuration/StandardSequences/data/FrontierConditions.cff"
  include "FWCore/MessageService/data/MessageLogger.cfi"
```

```
untracked PSet options =
{
  include "FWCore/Framework/test/cmsExceptionsFatalOption.cff"
  untracked bool wantSummary = true
  untracked bool makeTriggerResults = true
}

source = PythiaSource
{
  untracked int32 pythiaPylistVerbosity = 0
  untracked bool pythiaHepMCVerbosity   = false
  untracked int32 maxEventsToPrint      = 0
  untracked double filterEfficiency     = 1.

  PSet PythiaParameters =
  {
    # This is a vector of ParameterSet names to be read, in this order
    vstring parameterSets =
    {
      "pythiaUESettings",
      "processParameters"
    }

    include "Configuration/Generator/data/PythiaUESettings.cfi"

    vstring processParameters =
    {
      'MSEL=0         ! User defined processes',
      'MSUB(11)=1     ! Min bias process',
      'MSUB(12)=1     ! Min bias process',
      'MSUB(13)=1     ! Min bias process',
      'MSUB(28)=1     ! Min bias process',
      'MSUB(53)=1     ! Min bias process',
      'MSUB(68)=1     ! Min bias process',
      'MSUB(92)=1     ! Min bias process, single diffractive',
      'MSUB(93)=1     ! Min bias process, single diffractive',
      'MSUB(94)=1     ! Min bias process, double diffractive',
      'MSUB(95)=1     ! Min bias process'
    }
  }
}

include "Configuration/StandardSequences/data/Generator.cff"
include "Configuration/StandardSequences/data/Reconstruction.cff"
```

```
  include "Configuration/StandardSequences/data/Simulation.cff"
  include "Configuration/StandardSequences/data/MixingNoPileUp.cff"
  include "Configuration/StandardSequences/data/VtxSmearedGauss.cff"
  include "Configuration/StandardSequences/data/L1Emulator.cff"

  path p0 = {pgen} # generator information
  path p1 = {psim} # simulation
  path p2 = {pdigi} # digitization
  path p3 = {reconstruction_plusRS_plus_GSF} # reconstruction
  path p4 = {L1Emulator}

  include "Configuration/EventContent/data/EventContent.cff"

  module FEVT = PoolOutputModule
  {
    using FEVTSIMEventContent
    untracked string fileName = "MinBias.root"
    untracked PSet dataset =
    {
      untracked string dataTier = "GEN-SIM-DIGI-RECO"
    }
  }

  endpath outpath = {FEVT}

  schedule = {p0,p1,p2,p3,p4,outpath}
}
```

Appendix B

Statistics at the GenEvent-stage

	Absolute numbers			
	all η	$\|\eta\|<2.5$	$\|\eta\|<1.48$	$\|\eta\|<0.9$
Photons γ:	61,60	24,14	14,49	8,80
with p > 1GeV:	27,77	4,62	1,30	0,53
with 1> p > 0.5 GeV:	5,01	4,62	2,30	1,15
with 0.5 > p > 0.1 GeV:	9,10	10,88	7,50	4,68
$\pi^+/\ \pi^-$:	51,31	18,89	10,97	6,52
$K^+/\ K^-$:	6,24	2,15	1,20	0,70
K^0_S:	3,01	1,02	0,57	0,33
K^0_L:	3,03	1,03	0,57	0,33
π^0:	0,00	0,00	0,00	0,00
Neutrons n:	4,35	1,21	0,67	0,38
Protons p :	4,79	1,19	0,65	0,38
$e^+/\ e^-$:	0,75	0,29	0,17	0,10
$\mu^+/\ \mu^-$:	0,01	0,01	0,00	0,00
Strange Baryons:				
Λ:	1,33	0,37	0,20	0,11
Σ^+:	0,30	0,09	0,04	0,03
Σ^-:	0,28	0,08	0,04	0,02

Table B.1: Absolute numbers of status one particles in different $|\eta|$-ranges at GenEvent-stage

	Percentages			
	all η	$\|\eta\|$<2.5	$\|\eta\|$<1.48	$\|\eta\|$<0.9
Photons γ:	44,89	47,76	48,94	49,59
with p>1GeV:	27,77	9,14	4,40	3,01
with 1> p >0.5 GeV:	5,01	9,14	7,76	6,48
with 0.5 > p > 0.1 GeV:	9,10	21,53	25,34	26,35
π^+/ π^-:	37,40	37,37	37,04	36,76
K^+/ K^-:	4,55	4,25	4,07	3,96
K^0_S:	2,19	2,02	1,92	1,88
K^0_L:	2,21	2,04	1,91	1,88
π^0:	0,00	0,00	0,00	0,00
Neutrons n:	3,17	2,40	2,25	2,17
Protons p:	3,49	2,35	2,20	2,14
e^+/ e^-:	0,55	0,58	0,57	0,56
μ^+/ μ^-:	0,01	0,01	0,02	0,02
Strange Baryons:				
Λ:	0,97	0,74	0,66	0,65
Σ^+:	0,22	0,17	0,15	0,15
Σ^-:	0,20	0,17	0,15	0,14
X % are missing	0,16	0,14	0,13	0,12
No. of status one particles	1372088	505502	296046	177418
% of all status one p.	100,00	36,84	21,58	12,93

Table B.2: Percentages of status one particles in different $|\eta|$-ranges at GenEvent-stage

Appendix C

Additional charts and tables for the statistics of the simhits and process types of simhits

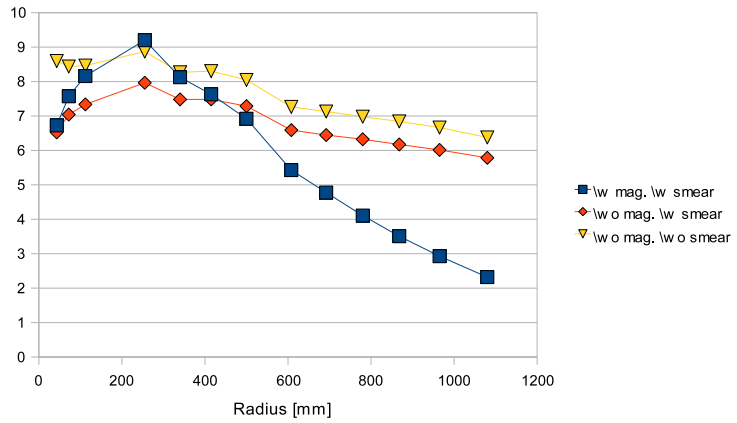

Figure C.1: The average number of hits with the process type "Primary" for three different regimes: 1. With magnetic field and smearing (as in the experiment), 2. Without smearing, with magnetic field, 3. without smearing and magnetic field

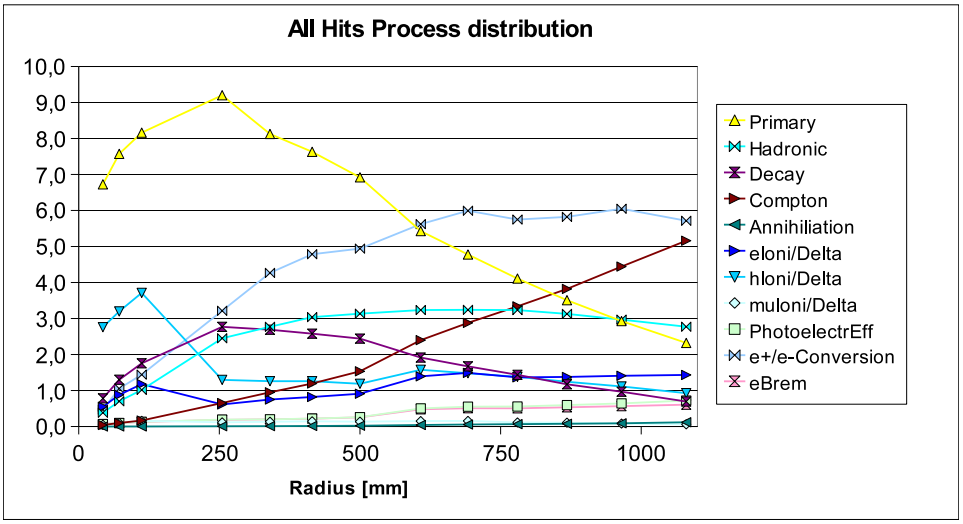

Figure C.2: The chart shows the origin of all simhits in the PXB, TIB and TOB according to the process type stored in the simhit-container

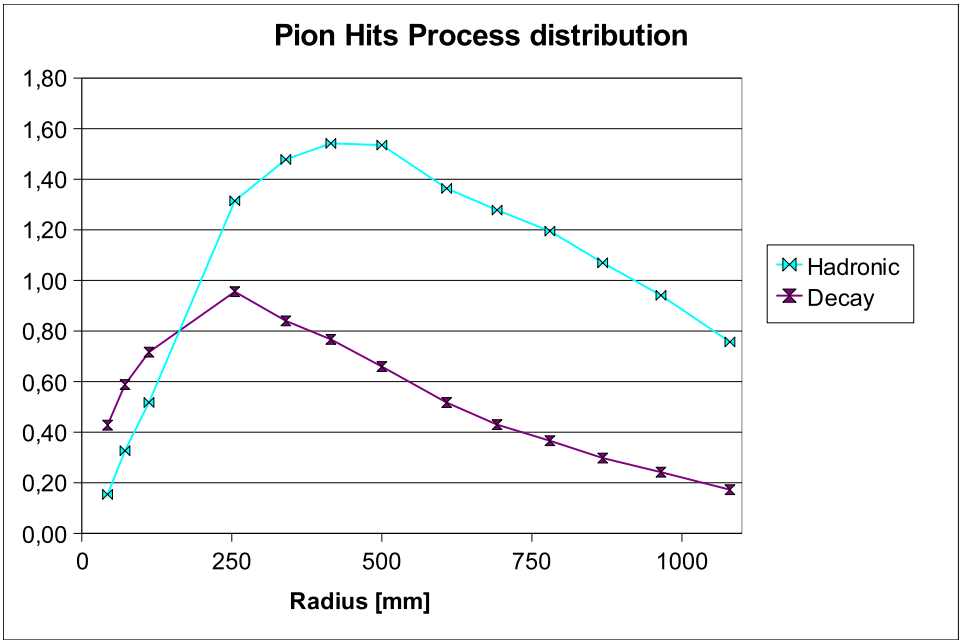

Figure C.3: Detailed chart of lower rate proceses causing pion hits

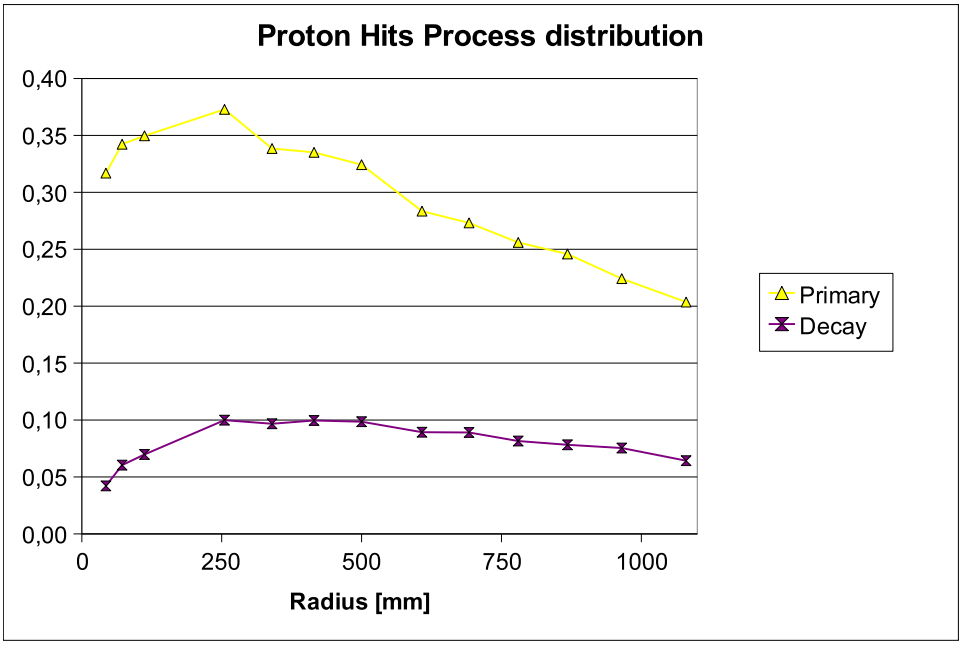

Figure C.4: Detailed chart of lower rate proceses causing proton hits

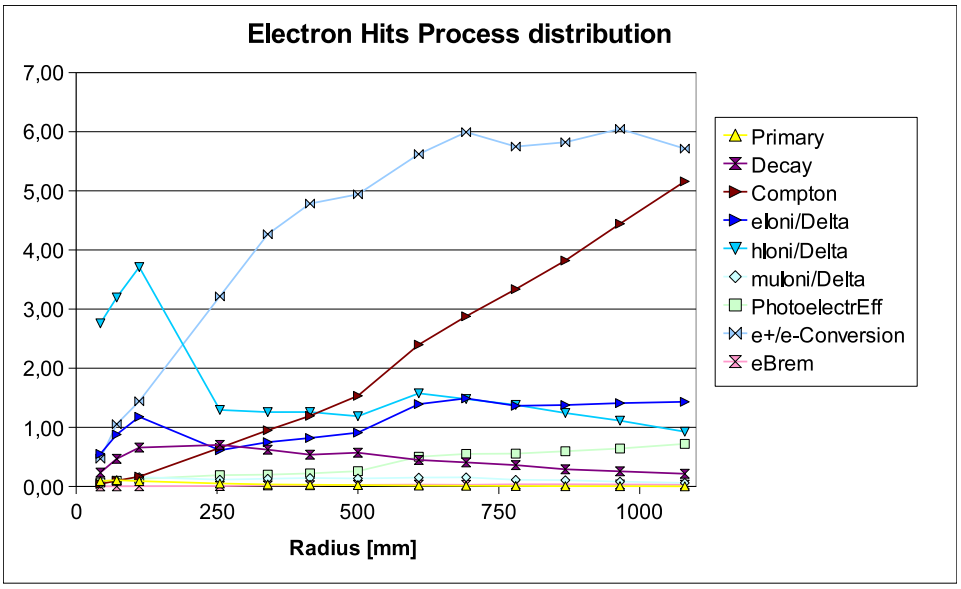

Figure C.5: Detailed chart of lower rate proceses causing electron hits